# Assessing dust impact on air quality using the global chemistry and transport model TM4-ECPL

Master thesis

**Student:**

Medea Zanoli

matriculation number: 3184237

date of birth: 17.04.1995

**Examiners:**

Mihalis Vrekoussis

Nikos Daskalakis

Academic year 2020-2021

Submission date: 27/04/2021

# Contents

# 1 Abstract

This study aimed at assessing the impact on air quality of natural dust in densely populated cities of the Mediterranean basin. In particular, we aimed at estimating the natural dust fractional contribution to daily exceedances of the EU PM10 limit, which is set to 50 $\mu g/m^3$ for 24h-averaged values of PM10 concentration..

In this study, we assessed the performance of a new model-based approach to determine the contribution of natural dust to the total PM load. The model of interest is the TM4-ECPL chemical transport model, which is available in two versions with different dust emissions schemes, one *online* and one *offline*. We propose the use of online emissions to make this method independent from measuring campaigns, which limit the time-range of study and rises the costs, bottom-up estimates, which inevitably lead to inaccuracies, and back-trajectory calculations.

Both versions of the TM4-ECPL have been succesfully validated for surface dust concentrations. A model weakness at modelling the surface PM10 concentration in the Mediterranean basin has been highlighted by this study. A surface PM10 concentration validation has been perfomed for the Mediterranenan area, revealing a general bad correspondance between the modelled and measured PM10 field along the basin.

The proposed method was used to calculate the number of exceedances and the corresponding fractional dust contribution in 6 Mediterranean cities, obtaining reasonable results. However, a further analysis would be needed to understand which atmospheric processes are at the basis of the PM10 overastimation in the basin, for example by validating the dust depostion fluxes, or by performing a second global validation with AOD fields to better understand the goodness of the modelled dust emissions.

## 2   Introduction

The world's large arid and semi-arid regions emit every year in the atmosphere great quantities of particulate matter in the form of natural dust, which, entrained by the winds, can travel thousands of kilometres far from their sources before being removed[1]. The major dust emissions sites of the planet are located in the Northern Hemisphere along the so-called Dust Belt, which extends from North Africa, across the Arabic peninsula to South and Central Asia [2] (see fig.1). The annual global dust emission is estimated to be around 1000-2150 Tg, accounting for the 45% of global aerosol emissions, most dust emissions coming from the Sahara-Sahel region (50-75 % of the total [1]). The annual cycle of dust in the atmosphere shows seasonal patterns: in the Sahara region dust emissions peak in Summer, while Asian deserts show a maximum in Spring[3]. From North Africa, the main transport routes follow the westerly winds towards Americas' coasts, carrying dust in the Caribbean and USA in Summer and in South America in winter [4], but intruding also in the Eastern Mediterranean basin during Spring [5],[6],[7] and in the Western part of the basin in Summer [8]. Asian dust travels eastwards, crossing the Pacific Ocean and reaching North America[1] (see fig. 2).



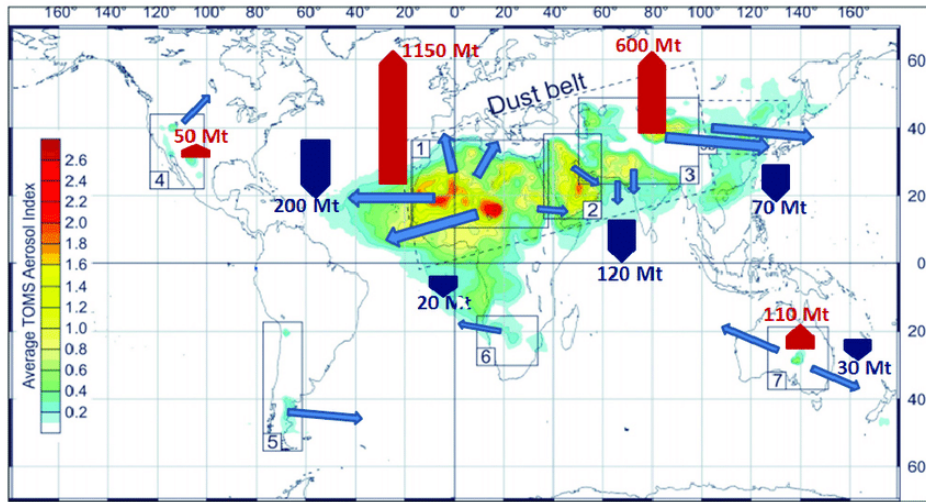Figure 1: *Major natural dust sources: (1) Sahara, (2) Arabia, (3) Asia, (4) North America, (5) South America, (6) Southern Africa, and (7) Australia represented in terms of the average TOMS Aerosol Index values. Natural dust main transport routes are indicated with light blue arrows. Red arrows depict emissions in Mt (= 1 Tg) from different areas and blue arrows deposition to the ocean. Taken from [2]*
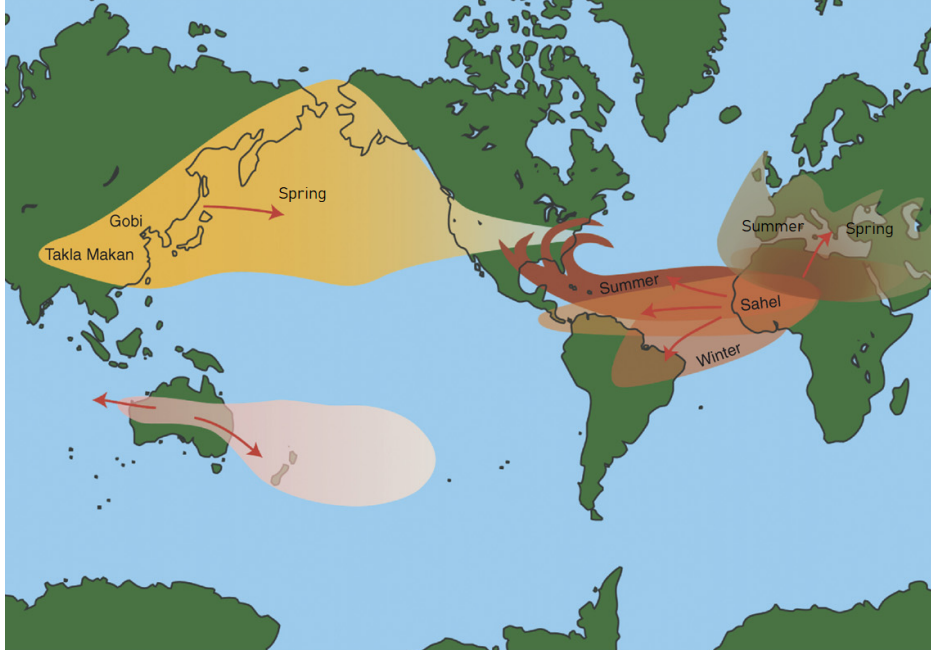
Figure 2: *Seasonality of the North African and Asian dust transport routes. Sahara-Sahel dust is carried to the Caribbean and USA from May to November, while between December and April the transport shifts to South America. Saharan dust transport in the Mediterranean basin peaks in Summer in its western region and in Spring in its eastern region. The Asian dust outbreak peaks between February and May. Taken and modified from [13]*

Mineral dust has significant effects on the Earth system, the climate and human health. It is reported to impact on the global radiation balance [9], on rain and droughts patterns [4], on the marine plankton population [10], the decline of coral reefs[11] and on the terrestrial primary productivity [12],[13]. Sand and dust storms can cause high concentrations of PM in the air over long periods, posing a hazard not only for the residents of the world's dryland but also for regions located downwind of the dust transport [2] (see fig.3). Suspended particulate matter (PM) was found to be correlated with an increase in the risk of respiratory diseases, cardiovascular complications and premature death [14],[15],[1]. In the African region dust and meningitis epidemics might be linked[18]. It has been shown [6] that during dust events the amount of deposited PM in the human lungs can be comparable to that experienced in heavily polluted urban areas. Natural dust was also proved to be a carrier for pathogenic microorganisms, such as fungi and bacteria [16][1],[2].
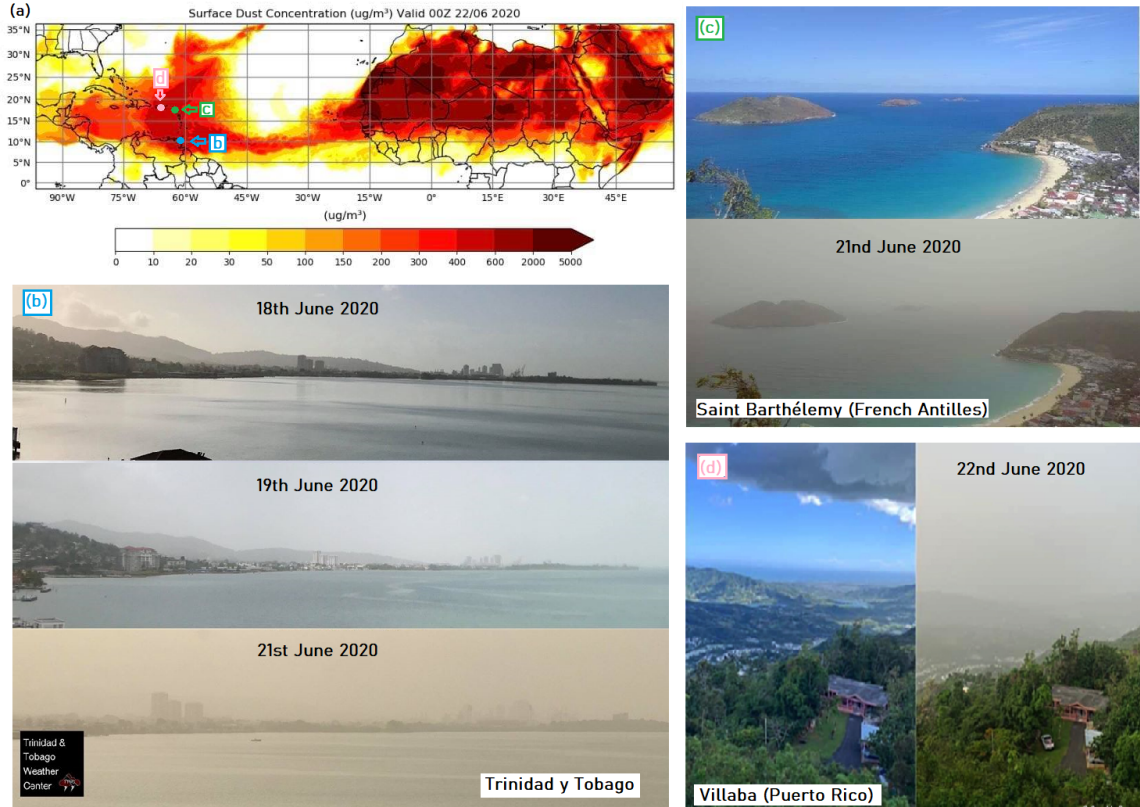
Figure 3: *(a) "Godzilla" dust storm reaching the Caribbean from North Africa on 22nd June 2020 as registered by NASA satellites. (b), (c), (d) Visibility conditions dramatically worsen with respect to normal conditions due to the high atmospheric dust load at different Caribbean locations.*

Dust emissions are highly sensitive to climate change and its emissions have risen considerably in the last decades after several centuries of constant trend [4], probably because of the unprecedented periods of droughts experienced in North Africa [17] and central Asia[1]. The ongoing desertification in many areas of the world will increase the future atmospheric dust load[16], making a better understanding of desert dust emissions and transport an issue of relevant importance today.

In the past years several studies have underlined the relevance of Saharan dust for air quality and air PM levels have raised concerns for public health. The World Health Organization in its guidelines for air quality has set limits for PM concentration, along with the European Union and the USA (see table 1 for values). African countries, which are between the most affected by natural dust, often have neither air quality legislation, nor infrastructures to monitor PM[22]. The study of natural dust transport

and its contribution to the total PM load has been particularly wide in Europe. The Mediterranean basin, which with its dry climate favours long residence times of suspended particles in the atmosphere, is particularly susceptible to dust events. Dust episodes were shown to regularly lead to peaks in $PM_{10}$, occasionally causing the exceedance of the daily legal $PM_{10}$ level fixed by the EU Ambient Air Quality Directives [8],[5],[7],[6],[23],[24], and in some case causing the 100% of the registered exceedances [5]. An exceedance can be exempted by the State Member if it is scientifically proved to be caused by natural events, such as volcanic emissions, seismic or geothermal activity, wild fires, strong winds or resuspension or transport of natural particles from dry regions. Thus, the study of the transport of natural dust from the world's dry regions and the estimate of its contribution to the total $PM_{10}$ is nowadays of particular interest for policymakers and scientists.

| institution | pollutant | concentration | averaging period | max. exc./year |
|---|---|---|---|---|
| EU | $PM_{10}$ | 50 µg/m$^3$ | 24 hours | 35 |
| | | 40 µg/m$^3$ | 1 year | n/a |
| | $PM_{2.5}$ | 25 µg/m$^3$ | 1 year | n/a |
| USA | $PM_{10}$ | 150 µg/m$^3$ | 1 year* | 1 |
| | $PM_{2.5}$ | 35 µg/m$^3$ | 24 hours | n/a |
| | | 12** µg/m$^3$ | 1 year* | n/a |
| WHO | $PM_{10}$ | 50 µg/m$^3$ | 24 hours | n/a |
| | | 20 µg/m$^3$ | 1 year | n/a |
| | $PM_{2.5}$ | 25 µg/m$^3$ | 24 hours | n/a |
| | | 10 µg/m$^3$ | 1 year | n/a |

Table 1: *Air quality standards for health protection according to the EU, USA, and WHO. *over a 3 years average, **primary standards for public health. For reference see [19] [20] [21]*

Various approaches have been used to estimate the contribution of dust to $PM_{10}$. Many studies make use of satellite images and back-trajectories to track the transport of natural dust [25],[5],[24],[15]. Nevertheless, the total atmospheric dust cycle cannot be fully captured by these methods [26] and the transit of an air mass transporting mineral

dust does not necessarily lead to an increase of $PM_{10}$ at ground level [23],[27]. Querol et. all in [8] proposed a statistical method [25] to quantify the daily African-dust $PM_{10}$ load by subtracting the $PM_{10}$ regional background from the $PM_{10}$ measured on a dust-day at a rural station. This method cannot be automatically applied to other areas of the world without a chemical validation with local data [23], but in some country it is not trivial to dispose of a proper network of rural stations which are far enough from urbanized areas to guarantee the absence of anthropogenic contributions to the measured $PM_{10}$ [23]. Other methods significantly rely on the chemical analysis filter samples collected during measuring campaigns [5],[23], making the method applicable to a limited time periods and costly. In Gerasopolous et. all.[5] strong time correlations are shown between high $PM_{10}$ load measured at both urban and remote locations and dust-enriched southerlies coming from North Africa. In the same study, the chemical characterization of $PM_{10}$ collected during several exceedance days showed the significant presence of crustal aerosols of dust origin.

A model-based approach was used by Mitsakou et. al in [6], in which the impact of mineral dust transport on the air quality of Greek urban areas was quantified using the SKYRON weather forecasting system coupled with an algorithm for the online calculation of atmospheric dust cycle [28],[26]. The simulated dust concentrations were compared with the $PM_{10}$ measured at several monitoring stations. Fitting a linear correlation between the simulated dust concentration and the total $PM_{10}$ measured at a station location, the percentage of dust in the total $PM_{10}$ concentration is given by the trend line's slope. However, a source of error in this method is that different sources of PM can alter the correlation factor, particularly in urban areas. Additionally, in this area of the basin the dust-rich southwester winds were shown to be correlated with temperature changes, which are proved to enhance urban pollution and thus affect the air PM concentration. [29],[7].

In this study, we propose a new model-based approach to determine the contribution of natural dust to the total PM load. The model used is the TM4-ECPL chemical transport model, in which a routine for online dust emissions calculation has been implemented by Tagen et al. in [30]. We propose the use of online emissions to make this method independent from measuring campaigns, which limit the time-range of study and rises the costs, and bottom-up estimates, which inevitably lead to

8

inaccuracies. This method also does not need the use of back-trajectories to identify dust-days. As the different $PM_{10}$ components, natural dust included, are treated individually by the model, it is possible to use the model output to do a speciation of the total $PM_{10}$ load. In this way, the fractional dust contribution to the total PM10 can be directly computed for any location from the model output. The same applies to any other PM10 specie modelled by the TM4-ECPL.

## 2.1 Current scientific questions related to dust

Natural dust is today a widely discussed topic in atmospheric science due to the great uncertainties of its effects on the Earth climate and its global budget. For example, the uncertainties on dust direct and indirect radiative forcing are so large that the very same sign of the forcing is still unclear[35], and understanding its contribution to the Earth global energy budget might be a challenge for future climate predictions. [34].

On the modelling side, global models which simulate the dust cycle show large differences between them, particularly when it comes to the simulation of dust depostion fluxes[60] and surface concentrations[36], which models usually reproduce within a factor of 10. Vertically integrated parameters, such as AOD, are generally better captured (usually within a factor of 2). Models also often fail at capturing the temporal and spatial distribution of the dust transport, capturing better the transport towards downwinds locations than remote ones[60]. A recent study[55] suggested that coarse-resolution models might be intrinsically inadequate to simulate the global dust cycle.

# 3   An overview on particulate matter

## 3.1   PM effects on human health

The term "particulate matter" (abbreviated PM) refers to the mixture of solid particles and liquid droplets which are suspended in the air. Particles with a diameter smaller than 10 µm are referred to as PM10, and when inhaled can penetrate deep into the lungs. As figure 4 shows, particles in the diameter range between 2.5 and 10 µm, such as coarse dust, can reach the bronchial regions of the lung, and accumulates mainly at pulmonary bifurcations of the bronchus. Particles whose diameter is smaller than 2.5 µm (PM2.5) can penetrate into the alveolar regions and get into the bloodstream [37].
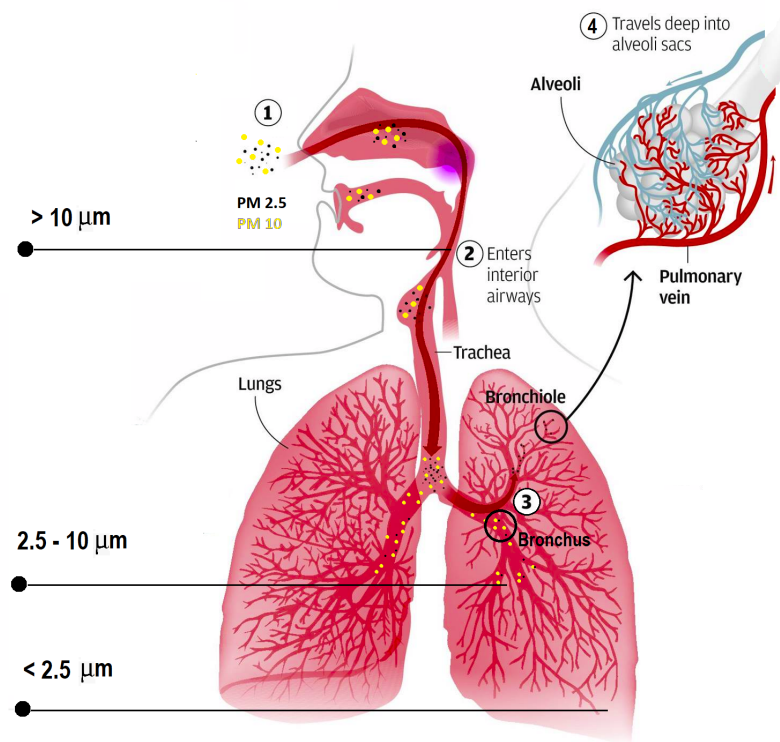


Figure 4: *PM10 and PM2.5 enters the respiratory system through the mouth and the nose (1), travel down into the thrachea (2) and penetrates the lungs. PM10 accumulates in the bronchus area (3), while PM2.5 can penetrate deeper into the alveolar region and get into the blood (4).*

The inhalation of PM has thus shown to be correlated with cardiovascular, cerebrovascular, respiratory diseases and, for long exposure time, cancer. High levels of PM10 in urban air has been shown to correlate positevily with an increase in hospital admissions and

natural mortality for cardio-respiratory complications [38]. Desert dust, being one of the major components of atmospheric PM10, poses a serious threat to health: the statistical association between PM10 and mortality has shown to be equally strong for desert-PM10 and non-desert PM10[38],[39]. Dust events can thus raise concerns of national authorithies of the affected countries, and protective measures need to taken to garantee the safeguard of public health on days affected by natural dust transport, for example by limiting anthropogenic PM10 emissions and adopting measures which limit the population exposure. Figure 5 shows an example of a national alert issued by the Trinidad y Tobago Weather Center during a sever dust outbreak in June 2020, attributing to this metereological event the maximum level of public health concern.
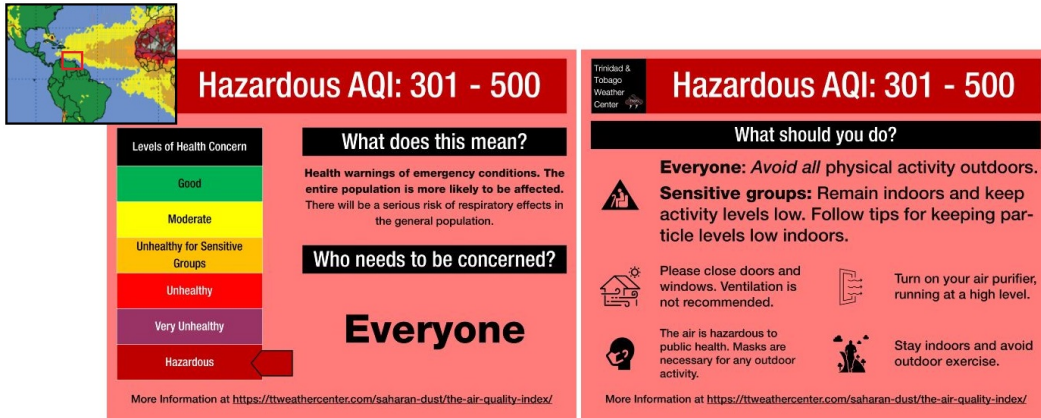


Figure 5:    *Trinidad y Tobago Weather Center alert to the population during an unprecedented Saharan dust outbreak in June 2020.*
*Source: https://ttweathercenter.com/an-unprecedented-saharan-dust-outbreak-for-tt/*

## 3.2   Dust size distribution

The diameter of atmospheric aerosols extends over four orders of magnitude, from a few nm to tens of $\mu$m. Their mass and volume distribution is characterized by two dominant modes: the *accumulation mode* in the $\sim$ 0.1 - 2 $\mu$m range and the *coarse mode* in the $\sim$ 2 - 50 $\mu$m range. Aerosols are classified between *fine* and *coarse* according to their diameter, the threshold diameter being 2.5 $\mu$m (*fine* if $d < 2.5\mu m$, *coarse* if $d > 2.5\mu m$). Coarse particles are usually produced via mechanical processes, such as wind entrainment and erosion in the case of natural dust. In terms of volume distribution, desert dust falls mainly in the coarse mode, with a small overlapping with the accumulation mode, while its number distribution shows a wide maximum around

0.03 $\mu$m. This means that, in terms of number, most dust particles fall in the fine and ultrafine regime, but most of their mass belongs to the coarse regime. As can be seen in figure 6, in terms of number distribution, a significant fraction of desert dust falls in a range which is hazardous to human health.
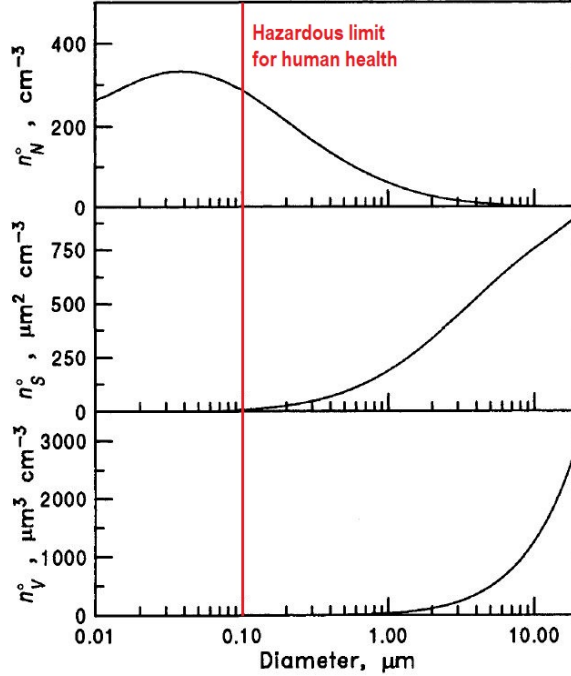


Figure 6: *Common desert dust number, surface and volume distribution*[40]

## 3.3   Emission, transport and deposition of natural dust

The movement of dust happens in three phases: entrainment from the surface (emission), transport and deposition [41](see figure 7).

Emissions are produced by erosion of the surface and wind entrainment. The forces acting on a dust particle at rest are its weight and the interparticle cohesion forces, which depends on the grain size, and the shear stress exterted by the wind on the surface, which depends on the surface properties and the wind speed [31]. In general, the amount of wind erosion is a function of different climatic factors, among which the soil erodibility, the surface roughness, the vegetation cover, and the effective precipitation, which is the amount of precipitation that remains in the soil after evaporation [41]. The wind speed is by convention measured at 10 m from the surface and the threshold value of minimum wind speed is often set to 6.5 m·s$^{-1}$ [40]. The vertical movement of dust can happen through different processes depending on

12

Figure 7: *Dust transport schematic: emission, long range transport by wind entrainment, dry and wet depositon. Taken from [44]*

the grain size: creep, saltation and suspension (see figure 8). The smallest particles ($<$ 60 µm [31]) are brought upward by turbulent eddies ("suspension") and if they reach the boundary layer can be transported over a long-range. The "saltat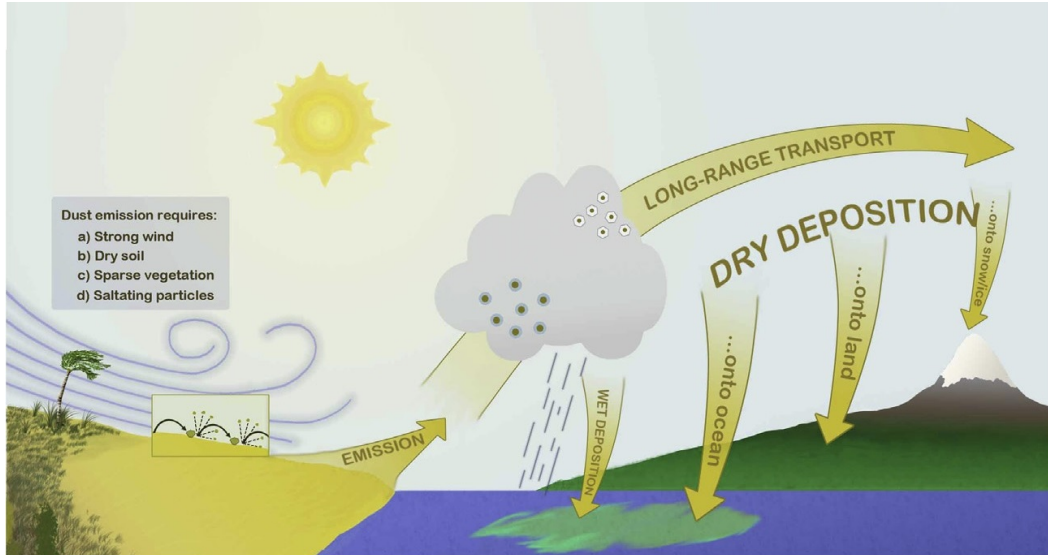ion" process refers to the ballistic motion of particles in the 70 - 500 µm range, which falling back on the surface cause the disintegration of soil aggregates and the emission of finer particles ("sandblasting"). The biggest and heaviest particles, which can not be lifted by the wind ($\sim$ 500 µm [43]), roll along the surface in a motion called "creeping" [31].

After dust is entrained by the wind, the finest particles (typically $\leq 10$ $\mu$m) can travel over long distances (often $\sim$ 5000 km or more [40]), while bigger particles tend to deposit near the source region. On average, the lifetime of a dust particle in the atmosphere is two weeks.

Dust deposition happens through dry or wet deposition. Dry deposition refers to the gravitational settling of aerosol particles over surfaces without precipitation processes being involved. Wet deposition comprises all removal processes which happens with the aid of precipitation. It can be divided in in-cloud scavenging, during which the aerosol falls to the ground with a rain droplet or ice crystal (weather because it served as a CCN or because it was dissolved in it), and below-cloud scavenging, in which the aerosol is mechanically brought to the surface by a falling rain drop.
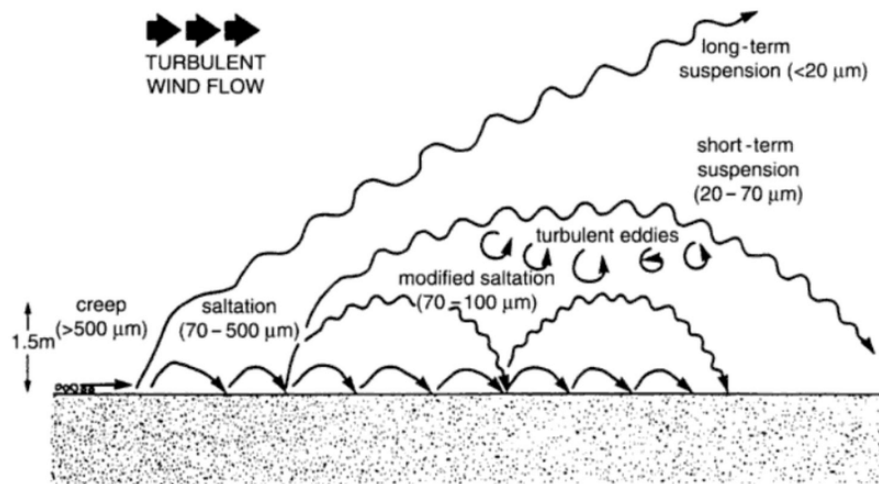
Figure 8: *Schematics of the main dust vertical trajectories due to wind shear stress. Taken from [43]*

# 4　Methods

## 4.1　Chemistry and transport models (CTM)

In this study, the state of the atmosphere is simulated using a Chemistry and transport models (CTMs). CTMs are a powerful tool to investigate the chemical compostion of the Earth's atmosphere. They can simulate the 3D chemical and dynamical processes that control the atmosphere evolution. Transport and chemistry of the modelled atmopsheric species are usually determined by solving a coupled system of continuity equations., which express the mass conservation of all $n$ chemical species. If the equations are solved in a geographically fixed frame of reference, the model is called *Eularian*, and the continuity equation can be written in its general form as:

$$\frac{\partial C_i}{\partial t} = -\mathbf{v} \cdot C_i + P_i(\mathbf{C}) - L_i(\mathbf{C}) \tag{1}$$

where $\mathbf{v}$ is the velocity field, which comes from the 3D metereological wind field, and $\mathbf{C} = (C_1, \,...\, , C_n)$ is the vector contaning the concentrations of the $n$ modelled atmospheric species. This equation expresses that the *local* change of the concentration of an atmospheric specie $C_i$ with time comes from three processes: the advective flux $\mathbf{v} \cdot C_i$, the total production rate of the $i$-specie $P_i$ and its total loss rate $L_i$. The advective flux is equal to the total amount of the $i$-specie transported into an atmospheric volume by the winds minus the total amount of the $i$-specie transported out. The production and loss terms $P$ and $L$ depends on the $\mathbf{C}$ vector because production and loss can be produced, for example, by chemical reactions of $C_i$ with the others $n-1$ species. The production term $P$ also includes emissions, which can be read by the model as an input from an external inventory or can be calculated by the model itself (in this case we speak of *online* emissions). The loss term includes all the processes that decrease the specie concentration, such as scavenging by precipitation and deposition.

### 4.1.1　Online and offline CTMs

CTMs can be divided between *online* and *offline* depending on whether the meterological fields are generated by the model itself or if they are imported into the model as an input, for example from an external metereological model. In the *online* approach, a

meteorological model is initially run, independently of the chemistry. The resulting meteorological fields are then used to calculate the chemistry and atmospheric transport. On the contrary, in the *online* approach, both chemistry and meteorology are computed at each model time step, and the chemical continuity equations are coupled with the conservation equations of metereological variables such as air mass, momentum, heat, and water[45]. In an online model, the chemistry can thus affect the meteorology and viceversa. Some information about atmospheric processes is lost when choosing an *offline* approach over an *online* one. In general, the choice of an *online* model allows a better characterization of atmospheric processes happening on a smaller timescale than the meteorology time step, as they reduces the time-averaging errors that arises when using an $offline$ metereology.

In this work, we differenciate between *online* and *offline* emissions schemes. Analogously to the metereology, *online* emissions refers to the fact that model can generate by itself the emissions of a certain specie, while we talk of *offline* emissions when the emissions are imported into the model as in input from external inventories. A substantial part of this work is the comparison between the use of an *online* and *offline* dust emission scheme.

The TM4-ECPL is an *offline* model because the meteorological data are read from the ECMWF model. However, we might sometimes refer in this document to an *online* version of the TM4-ECPL model, referring to the version of the TM4-ECPL which uses an *online* dust emissions scheme. In order to avoid ambiguity, in this work the terms *online* and *offline* always refer to the used dust emission scheme.

## 4.2 The TM4-ECPL model

The TM4-ECPL is a 3D eulerian global CTM (see figure 9). It simulates the emissions, the chemistry, the transport and removal processes of 146 atmospheric tracers in the offline version, and 220 in the online one [46]. The atmosphere is compartimentalized in boxes and the tracers transport between adjacent cells is calculated in a fixed frame of reference. The horizontal gridding is done along the meridians and parallels. TM4-ECPL allows the user to decide between a coarse resolution of $6° \times 4°$ and a finer resolution of $3° \times 2°$. In the vertical direction the discretization is given by 34 hybrid

pressure levels calculated as:

$$p(\phi, \theta, z) = a_t(z) + b_t(z) * p_{surf}(\phi, \theta) \tag{2}$$

where $a_t$ and $b_t$ are constants and $p_{surf}(\phi; \theta)$ is the surface pressure at the location with latitude $\phi$ and longitude $\theta$, between the surface and the top level set at $0.1hPa$. All chemical reactions are calculated at equilibrium inside the boxes, and the boxes are connected between them through the air mass transport. Fast-reacting species (e.g, OH radicals) are not transported between boxes, but react with the species which are transported into the box and their concentration in each cell varies according to thermodynamic equilibrium calculations.



Figure 9: *Representation of how the TM4-ECPL model divides the atmosphere, the horizontal and vertical gridding specifications and some of the main model timesteps.*

### 4.2.1 The metereology

The metereology is imported as a model input from the ERAInterim meteorological data of the European Centre for Medium-Range Weather Forecasts (ECMRF). The metereology fields include wind speed and wind direction, surface pressure, temperature, humidity, height of clouds, and rainfall. The metereological input is imported every 3 hours and assimilated where observations are not available. As a consequence, the model cannot capture rapidily changing events, such as rapid dust outbreaks.

### 4.2.2 The emissions

The TM4-ECPL reads anthropogenic and natural emissions from different inventories, with various spatial and temporal resolutions, ranging from daily to monthly depending on the dataset. In the case of offline dust emissions, the emissions are imported from the AEROCOM dataset with a daily temporal resolution [60].

In the case of online dust emissions, emissions are calculated by the model according to an online dust emissions scheme as explained in the section "The online emissions scheme".

### 4.2.3 The model steps

At the beginning of the simulation, a previously calculated state of the atmosphere is read by the model to set the atmosphere initial conditions. The model then reads the meteorology input. Each time a new meteorology is read, the model performs the following steps:

1. update the tropopause height

2. calculate tracers rainout

3. calculate $NO_x$ emissions from lightening

4. determine the new convection matrix

5. calculation of vertical air fluxes between cells

This preliminary part is not dependent on the tracer properties. The simulation then proceeds in the following order:

1. **Emissions**: Emissions are imported from pre-existing inventories

2. **Advection**: only long-lived tracers are subjected to advection

3. **Chemistry**

4. **Wet deposition:** the model calculate both in-cloud and below cloud scavenging according to the tracer type. All aerosols, including dust, belong to a one unique type.

5. **Dry deposition:** it applies to transported species only. The model calculate the surface resistance according to the tracer type.

The model gives as output the monthly averaged concentration of each of the simulated tracers in each grid cell. At the end of each month, the final concentrations are saved and used as initial condition for the successive month. Figure 10 shows a flowchart of the TM4-ECPL model.
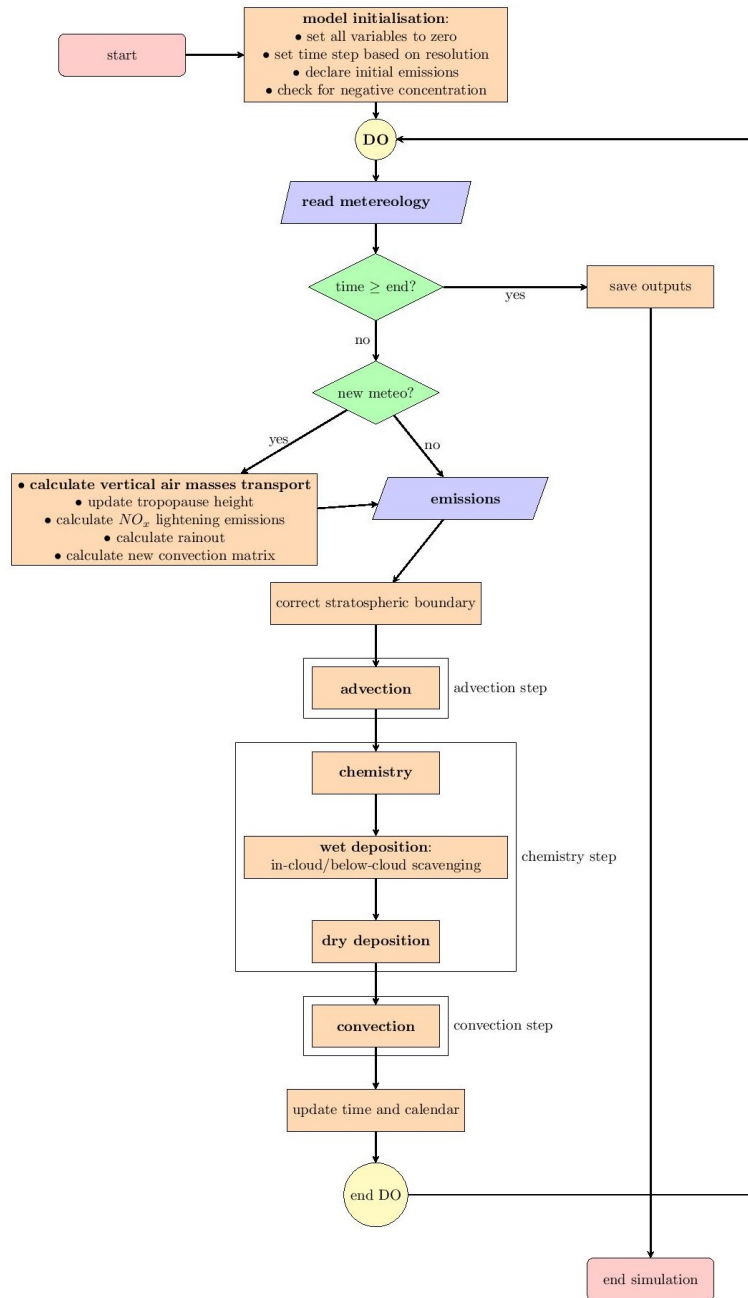


Figure 10: *Simplified schematics of the physical and chemical processes as modelled in TM4-ECPL*

### 4.2.4 The PM10 speciation

An element of novelty in our approach to find dust exceedance is the PM10 speciation. In the TM4-ECPL model, the different components contributing to the total PM10 load are simulated individually. The total PM10 concentration in each gridbox can thus be calculated by summing up the single atmospheric species belonging to this size range. Natural dust, divided in fine and coarse mode, is included in the summation, so that its fractional contribution to the PM10 can directly be calculated from the model output. In table 2 we report the species contributing to PM10 in the version od the model using *online* dust emissions. The species are regrouped in 5 categories: inorganic aersols, organic aerosols, biogenic aerosols, natural dust and sea salt.

| Atmospheric tracers | Category |
|---|---|
| Sulfate(SO4), Ferrihydrite(FeOH3), Ammonium (NH4), Nitrate(NO3), Inorganinc Phosphorus from biomass-burning and forest fires, Iron from biomass-burning and forest fires | Inorganic aerosols |
| Methanesulfonate (CH3O3S⁻), Marine Amines, Black Carbon, Organic Phosphorus from sea-salt, biomass-burning, primary biogenic particles and volcanic eruption, Alpha-Pinene, Beta-Pinene, Toluene, Xylene, Isoprene, Glyoxylic acid, Oxalic Acid, Marine Primary Organic Carbon | Organic aerosols |
| Bacteria, Fungal Spores, Pollen | Biogenic aerosols |
| Dust (coarse and acc. mode) | Natural dust |
| Sea Salt (coarse and acc. mode) | Sea Salt |

Table 2: *Atmospheric tracers modelled by the TM4-ECPL which participate in the PM10 load*

## 4.3 The online emissions scheme

In thi section we explain throughly the functioning of the online dust emission scheme used by the TM4-ECPL.

The used online dust emissions scheme was developped by *Tagen et al.* [30] based on the work of *Marticorena and Bergametti* [31], improved by *Heinhold at al.* [32] and adapted to read the ECMWF fields by E. Vignati.

New dust emissions are calculated for each surface gridbox at each metereology timestep (3 hours). Dust emissions are calculated based on semi-empirical relationships which take into account surface parameters and the meteteorology.

The emission of dust depends on the particle size distribution of the soil and is limited by vegetation, shrubs, snow cover and soil moisture. If these parameters are known for each gridbox and the metereology is taken into account, the dust emission from each gridbox can be calculated at each model timestep.

### 4.3.1 The vegetation type and snow cover

The distribution of vegetation types and cover is imported from the equilibrium terrestrial biogeography model BIOME4 [47] (see figure 11). BIOME4 can assess the biome type over a 0.5° gridbox depending on the monthly mean temperature, the precipitation, the net radiation, and the soil type. The world's biomes are schematized in 27 types. Seasonal and annual change of vegetation cover is estimated from monthly satellite observations as the fraction of absorbed photosynthetically active radiation (FPAR). Empirically, the dust source area of a gridbox is considered to depend linearly on the FPAR, being maximum when FPAR = 0 and zero if FPAR > 0.25. Girdcells with FPAR > 0.25 are considered as grass-dominated biomes, which do not produce dust.

In the model, the effective area $A_{eff}$ which produces dust emissions is calculated as:

$$A_{eff} = 1 - \frac{1}{25} \cdot [FPAR(max_{ann}) \cdot f_{shrub} + FPAR(month) \cdot f_{grass}] \qquad (3)$$

Where $f_{shrub}$ and $f_{grass}$ are the fractional contribution of shrubs and grass for each biome type, and $FPAR(max_{ann})$ is the maximum observed value of FPAR throughout the year. Thus the presence of shrubs and grass limit the dust production, lowerig it to zero when the the gridbox is totally covered with vegetation (corresponding to FPAR= 0.25).

Daily snow cover is imported from the European Centre for Medium Range Weather

Forecast (ECMWF) reanalysis (ERA) data. Snow-covered and wet areas are excluded in the dust emissions calculation.The soil moisture is also calculated by BIOME4.
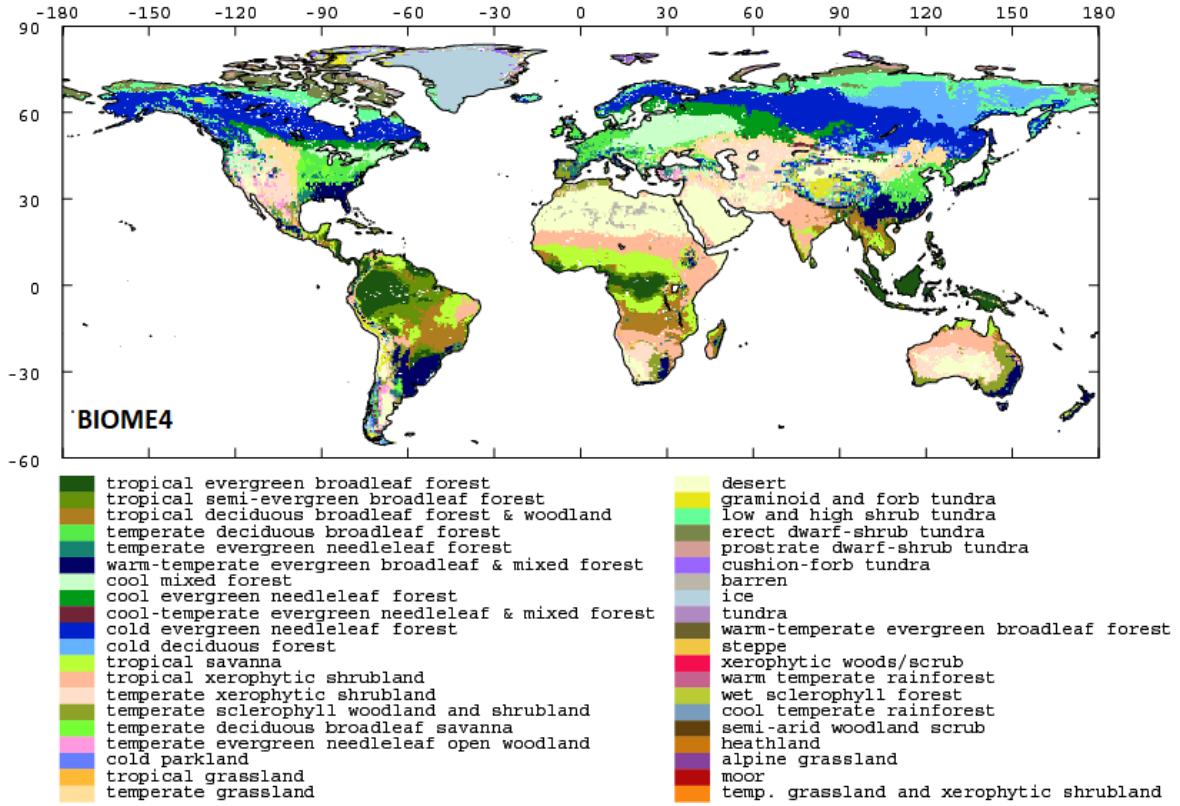


Figure 11: *BIOME4 reproduction of the distribution of the world potential natural vegetation for modern climate condition. Image from the Paleoclimate Modelling Intercomparison Project Phase II.*

### 4.3.2 The soil texture and size distribution

The soil texture class global estimated is taken from the United Nations Educational, Scientific, and Cultural Organization soil map of the World of the Food and Agriculture Organization [48], which categorize the superficial dominant soil texture with 0.5°x0.5° resolution. For dust emission, in the used scheme four populations of soils are considered: clay, silt, medium/fine sand and coarse sand. The soil size categories are fine, medium, coarse, or mixtures of these. In the emission scheme 12 sub-categories are included, given by coarse, medium, fine, and mixtures of these. For each type is defined a typical particle size distribution and the saltation efficiency $\alpha$. The size distribution in the model is calculated over 4 bins lognormally distributed between 0.1, 0.3, 0.9, 2.7, 8, 24 $\mu$m. In this model, particles whose radius is bigger than 24 $\mu m$ are neglected, as
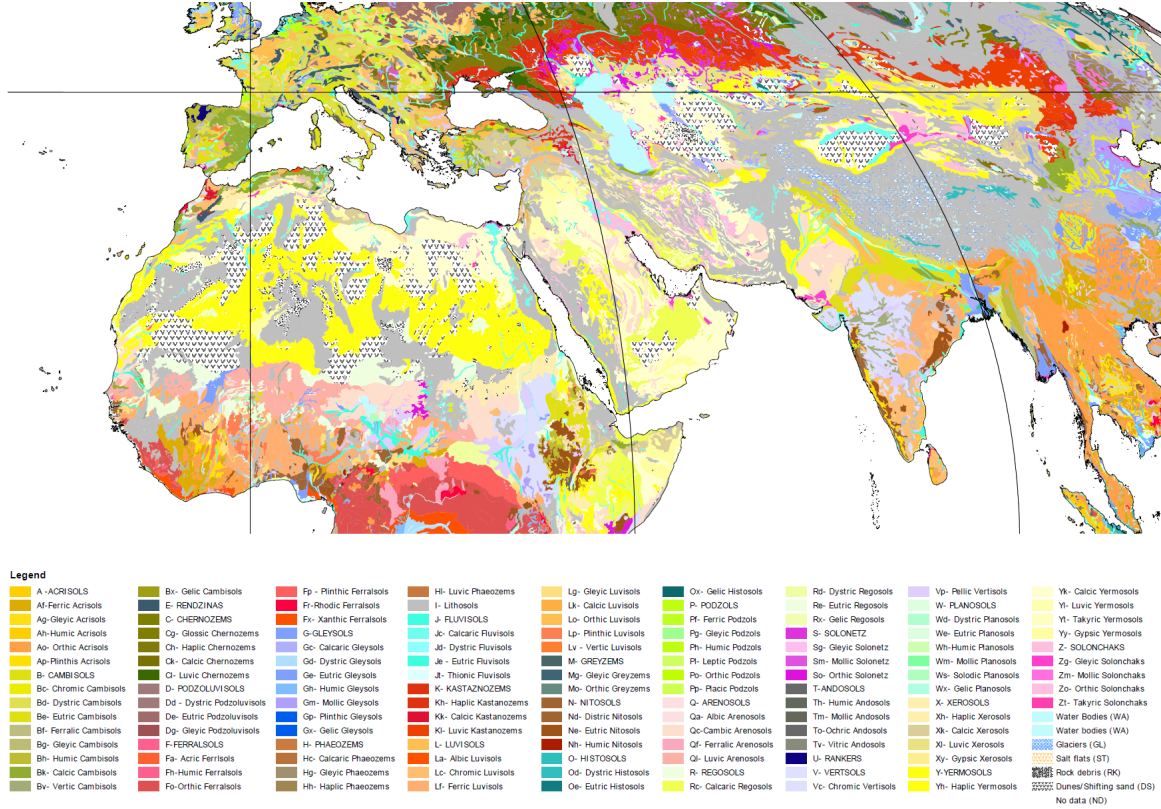
Figure 12: *A detail of the FAO soil map over the world "dust belt". Areas with white background and black pattern are dunes and sand. Available on the FAO soils portal: http://www.fao.org/soils-portal/data-hub/soil-maps-and-databases/en/*

it was shown that their contribution to long-range transport is insignificant[32]. The dust emissions fluxes calculated by the scheme are then grouped in two log-normal modes (accumulation mode and coarse mode).

### 4.3.3 The wind speed

The wind fields are imported as part of the ERAInterim metereological data. Dust emissions are calculated based on the wind speed at 10 m from surface.

Aeolian erososion can happen when the wind reaches a certain threshold velocity, which varies depending on the particle size and density. Theorethically, the dust wind entrainment is reached when the aerodynamic forces surpasses those of gravity and inter-particle cohesion. From this condition, the theoretical threshold wind speed $U_t^*$ is given by[31]:

$$U_t^* = A \cdot \left( \frac{\rho_P\, g\, D_P}{\rho_A} \right)^{\frac{1}{2}} \tag{4}$$

Where $\rho_P$ and $D_p$ are, respectively, the particle density and diameter, $g$ is the gravitational acceleration, $\rho_A$ is the air density and A an empirical parameter depending on the friction Reynolds number. In reality, the calculation of $U_t^*$ has to take into account cohesive forces (neglected in eq- 4) and changes for different regimes of the Raynolds number. In the online scheme, the parametrization of $U_t^*$ is given by the semi-empirical expressions proposed by *Marticorena and Bergametti* [1995][31]. The overall observed dependency of $U_t^*$ over the particle diameter is represented in figure 13. It can be noticed that the optimal diameter for mobilization lies between 60 and 100 µ$m$. These particles play a key role to mobilize smaller particles by saltation processes.
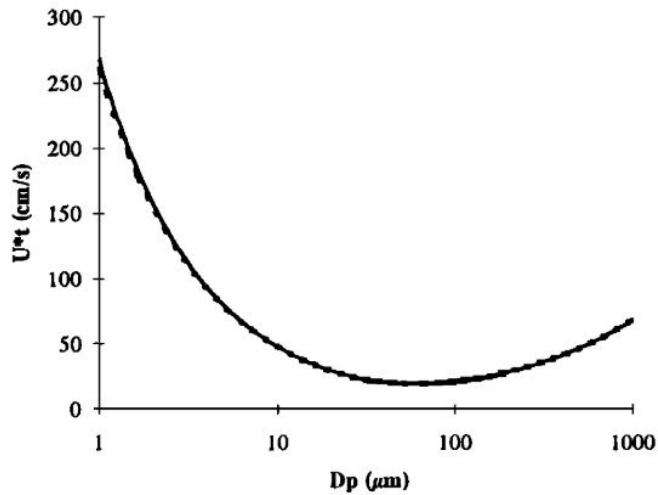


Figure 13: *Relationship between the wind threshold velocity $U_t^*$ and the particle diameter*

The friction velocity $U^*$ is calculated using a formulation based on the concept of roughness lenght $z_0$ [32],[33]. The roughness lenght $z_0$ is the typical lenght scale characterizing the loss of wind momentum due to roughness elements[31]. The vertical profile of the wind-speed $U(z)$, $U^*$ and $z_0$ are related under adiabatic conditions by the equation:

$$U(z) = \frac{U^*}{k} \cdot ln\left(\frac{z}{z_0}\right) \tag{5}$$

where $k$ is the Karman constant. In the TM4-ECPL emission scheme, 5 becomes, rearranged for $U^*$:

$$U^* = U_{1st} \, k \cdot ln\left(\frac{z_0}{z_{1st}}\right) \tag{6}$$

where $U_{1st}$ is the wind speed in the first model layer and $z_{1st}$ is the layer mid-height.

The model calculates the $z_0$ field as an input from remote seinsing data. The roughness of the surface is calculated as a function of the surface reflectance measured by the Polarization and Directionality of the Earth Reflectance (POLDER-1) sensor[32].

The wind with speed $U^*$ exerts on the surface an overall shear stress of[31]:

$$\tau = \rho_A \cdot U^{*2} \tag{7}$$

The shear stress is partitoned between roughness elements (such as shurbs and vegetation) and the bare surface[31]:

$$\tau = \frac{W_R}{S} + \frac{S_B}{S}\tau_s \tag{8}$$

where $S_B$ is the bare surface and S the total surface, $W_R$ is the force excerted over the roughness elements and $\tau_S$ is the residual stress acting on the bare surface. We thus see that the presence of the roughness elements protects the surface from the wind shear, and reduces dust emissions.

### 4.3.4  The dust production

If the friction velocity $U^*$ reaches the threshold value $U_t^*$, a dust flux is produced and transported vertically by the winds. Experimentally, the mass of particles M mobilized by the wind stress is proportional to the difference between $U^*$ and $U_t^*$ [31]:

$$M \approx \rho_a(U^* - U_t^*) \tag{9}$$

From figure 13 we see that particles between 60 -100 μm are the more easibly mobilized, but due to their size they tend to rapidily gravitatonally settle. The intermidiate process of saltation is essential for dust production: larger particles, falling down on the surface in ballistic motion cause the disintegration of soil aggregates and the emission of finer particles ("sandblasting"), or break down themselves in smaller fragments. The typical mean pathlenght of the mobilized particles is [31]:

$$L \propto \frac{(U*+U_t^*)^2}{g} \tag{10}$$

The smallest particles ($< 60$ μm) are then brought upward by turbulent eddies ("suspension") and if they reach the boundary layer can be transported over a long-range [31]. The
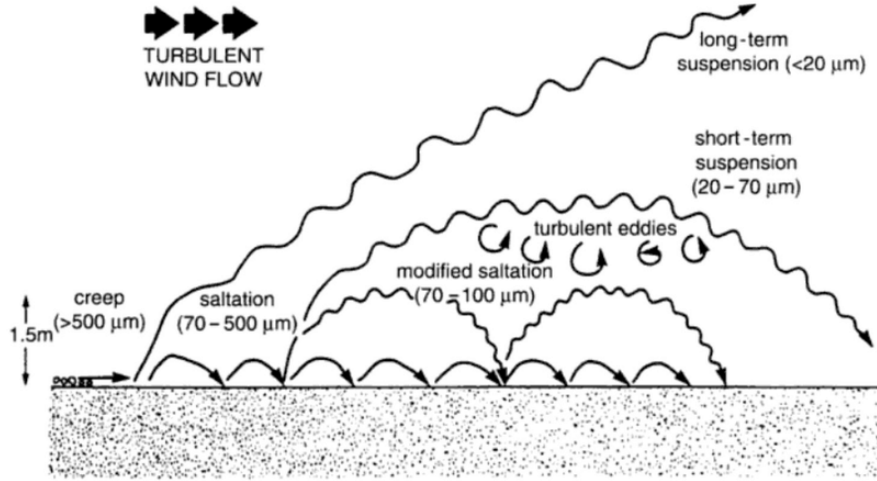
Figure 14: *Schematics of the main dust vertical trajectories due to wind shear stress*[42]

processes leading to dust production are schematized in figure 14. In the calculation of the dust fluxes the vertical flux of dust $F_v$, made of fine particles produced by saltation, is calculated as a fraction of the horizontal flux $F_h$ of creeping and saltating bigger particles. The horizontal flux can be estimated as:

$$F_h = M \cdot L \tag{11}$$

which putting toghether 9 and 10 leads to:

$$F_h = C \frac{\rho_a}{g} U^{*3} \left(1 + \frac{U_t^*}{U^*}\right) \left(1 - \frac{U_t^2}{U^{*2}}\right) \tag{12}$$

Where C is an experimental constant. In the model, this equation is approximated with:

$$F_h = \frac{\rho_a}{g} U^{*3} \cdot \sum_i \left[\left(1 + \frac{U_t^*(D_{pi})}{U^*}\right)\left(1 - \frac{U_t^*(D_{pi})^2}{U^{*2}}\right)\right] \Delta s_i \tag{13}$$

where the index $i$ runs over the particle size bins, ($D_{pi}$ is the particle diameter corresponding to the bin $i$, and $\Delta s_i$ is the relative surface area covered with particles belonging to the size bin. The vertical flux $F_v$ is considered proportional to the horizontal one:

$$F_v = \alpha F_h \tag{14}$$

where $\alpha$ is the saltation efficiency, which depends on the soil texture.

## 4.4 Online - offline dust emission scheme comparison

In this section we present the raw comparison between the dust concentration field produced by the two dust emissions schemes. The TM4-ECPL was run in 3°x2° for the years 2000 - 2017, once using the offline dust emissions scheme and once using the online dust emissions scheme. In figure 15 it is shown the relative change of the simulated superficial dust concentration $C$ when changing from the offline to the online emission scheme, calculated as:

$$change = \frac{C_{online} - C_{offline}}{C_{offline}} \cdot 100 \tag{15}$$
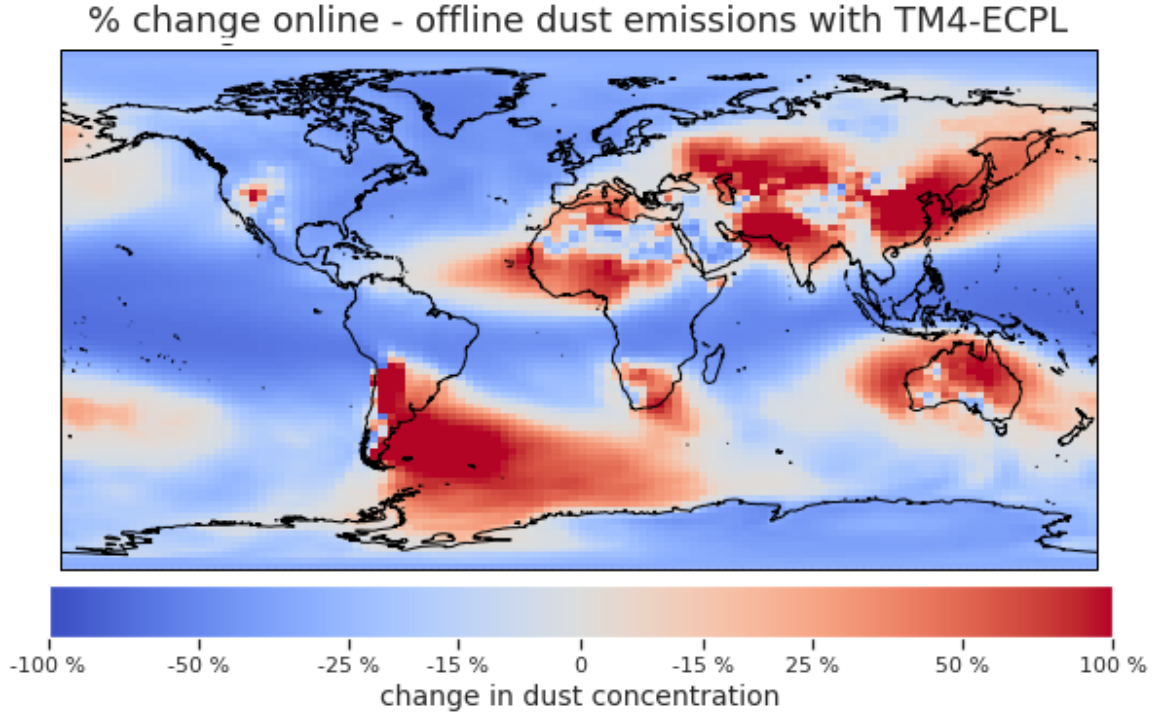


Figure 15: *Change in superficial dust concentration calculated as in 15, averaged for the period 2000-2017*

Figure 15 shows that the use of online emissions leads to significant changes in the superficial conecentrations of dust near the sources. We can observe a general decrease in the dust concentration in central Sahara and the Arabian peninsula, but also a significant increase in the Sahel area, Australia, central Asia, South Africa and South America.

# 5 Validation of the dust emission schemes

Both versions of the model, TM4-offline and TM4-online, have been validated against a dataset of dust observations performed between the years 2000 and 2017. We chose to exclude observations previous to the year 2000 because the process of dust emissions depends on characteristics of the surface, such as the vegetation cover and the soil erodibility, which varies over time and which can change considerabily over a decade. For this reason, the fact that a model performs well in reproducing the dust emission and tranport of 30 years ago is not representative of how the model would perform today.

However, the largest datasests of surface dust concentration measurements available remounts to the decade between 1980 and the mid-1990, during which 20 sites managed by the Rosenstiel School of Marine and Atmospheric Science at the University of Miami were active measuring monthly dust concentration [50],[51]. This datasets have been largely used in literature to validate model-simulated dust-concentrations[60],[55],[52]. Nevertheless, we decided to exclude most of these measurments in our validation and rely only on more recent observations.

To perform the validation, we run the models with spatial resolution 3°x2° and with a monthly output. This means that for each model grid, the model gives as output the monthly average of the dust concentration within the grid. We compared the observed monthly measurement of dust concentration (or the monthly average of the observations, where the observations had a finer temporal resolution), with the modelled dust concentration at the location of the station.

## 5.1 Description of the datasets

Our dataset is composed of 8 ground-based stations. The position of all stations is plotted in figure 16. Figure 16 reports also the average dust concentration field simulated by the online version of the TM4-ECPL model for summer 2006 (June, July, August), to make easier to viasualize the position of the stations with respect to the main dust emission regions and transport routes. All stations are located in key positions to study Saharan dust emissions and trasnport: the four african stations (M'Bour, Bambey, Cinzana, and Banizoumbou) are located on the edge of the major

28

natural emission region in the Sahel area, the american stations (Miami, Barbados and Cayenne) are situated downwind the atlantic transport, and Agia Marina is on the transport route crossing the Mediterranenan.
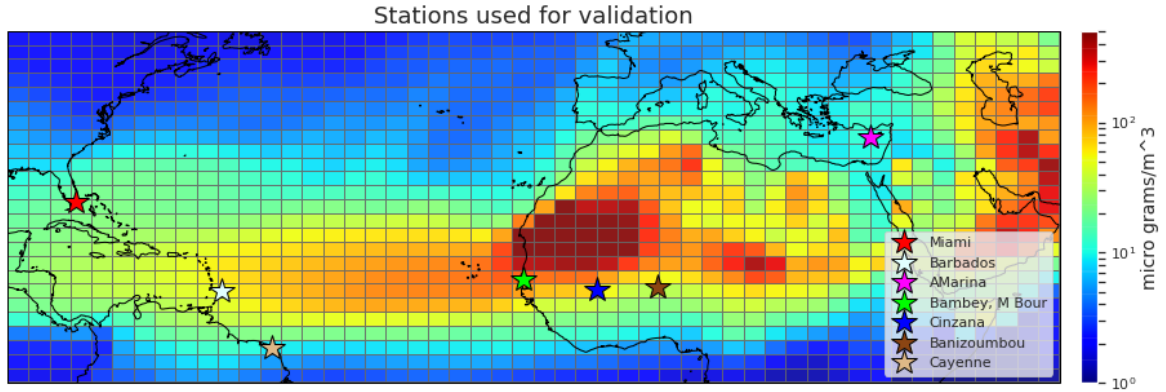


Figure 16: *8 stations used for the model validation, plotted over the dust concentration field simulated by the online version of the TM4-ECPL model for the summer 2006. Note that the two stations M'Bour and Bambey are so closed that they result superimposed on the map. The black grid correspsponds to the model gridding in 3°x2° resultion*

### 5.1.1 Miami and Barbados

The stations of Miami (25° 45'N, 80° 15'W) and Barbados (13° 6' N, 59°37 W) are part of the dust monitoring network of the Rosenstiel School of Marine and Atmospheric Science. They are both located downwind the dust transport pathway across the Atlantic Ocean from the Sahara-Sahel region. At both station the air masses coming from the open sea to the east are drawn into filters with high efficiency for dust [53]. Filter are then burned and the mineral dust load can be inferred from the ash residue weight, the multiplicative factor accounting for losses being 1.3. These measures have a standard error of $1 \pm 0.1$ $\mu g/m^3$ for concentrations below $\mu g/m^3$, and of $\pm$ 10 % for higher concentrations. These data are made publicly available by the Univeristy of Miami (see

`https://scholarship.miami.edu/discovery/fulldisplay/alma991031447546702976/`
`01UOML_INST:ResearchRepository`)

### 5.1.2 Cayenne

The station of Cayenne (4.95° N, 52.31 ° E) is located on the shores of the French Guyana, also downwind of the Atlantic dust transport pathway. For this location, we used the dust concentration timeserie calculated by J. M. Prospero&all (2020) in their paper "Characterizing and Quantifying African Dust Transport and Deposition to South America: Implications for the Phosphorus Budget in the Amazon Basin"[58]. In this study, the dust load is calculated by substracting a regional background from the $PM_{10}$ concentrations measured by the ATMO-Guyane nonprofit organization. The obtained dust concentration timeserie was successfully validated with the MERRA-2 model. Data can be obtained by personal correspondance with Prof. J. M. Prospero.

### 5.1.3 Agia Marina

The station of Agia Marina (35 °N, 33.06 ° W) is located on the island of Cyprus, in a strategic position to measure the dust transport in the East Mediterranean basin. In this dataset, the dust concentration is calculated from measures of PM load using the the methodology developed by Escudero & all[25]. The dataset was made available by Prof. Mihalis Vrekoussiss.

### 5.1.4 M'Bour, Bambey, Cinzana, and Banizoumbou

The stations of M'Bour, Bambey, Cinzana, and Banizoumbou belong to the Sahelian Dust Transect monitoring network [54] and are located in the semi-arid region of western Sahel, on the edge of one of the major dust emission regions. These stations, which are almost latitudinally aligned around 13°-14° N, lie along the transport route of African dust across the Atlantic Ocean to the American coasts. These stations record concentrations of aerodynamic $PM_{10}$ [55] and meterological parameters, such as wind speed and direction, every 5 minutes. Even if the quantity measured is not directly dust concentration, a good-enough estimate of it can be inferred from these measurements. To get a value from dust concentration from these observations, the original data were postprocessed in three steps: they were filtered for wind direction, selecting only those measurements taken when the wind was coming from dust-rich regions [57], the aerodynamic diameter was corrected for geometric diameter[55], and a rolling mean was applied to exclude outliers. These postprocessing steps are described

in the following section.

### 5.1.5 Data postprocessing of African stations

The first postoprocessing step was to filter the data for wind direction, selecting only those measurements taken when the wind was coming from dust-rich regions [57]. For observations taken in M'Bour (Senegal, 14.39° N, 16.96° W) and Bambey (Senegal, 14.70° , 16.47° W), we retained data corresponding to the wind direction spanning from 30° to 150° to exclude air masses rich of sea-salt and pollutant from the sea and the city. For the stations of Banizoumbou (Niger, 13.54° N, 2.66° E) and Cinzana (Mali, 13.28° N, 5.93° W), we filtered out southerly air masses coming from the sector 90°-270° during the dry season (October to April), to avoid the interference of biomass burning aerosols.

The correction to aerodynamic to geometric diameter was performed following the method develloped by J. F. Kok & all.[55]. As calculated by Huang et al., 2020[56], a geometric diameter of 10 $\mu m$ corresponds to an aerodynamic diameter of 6.8 $\mu m$. To compare the output concentration field of our simulation, in which $PM_{10}$ is calculated with respect to geometric diameter, with the oservations, only the fraction of our model output corresponding to $PM_{6.8}$ (geometric) should be taken into account. Since the TM4 for dust divides only between fine mode ($PM_{2.5}$) and coarse mode ($PM_{10}$), only the coarse mode bin is affected by the correction. Following J. F. Kok & all, the fractional contribution of the modelled dust concentration in the coarse mode to the aerodynamic $PM_{10}$ $FC_{aeroPM10}$ can be calculated as:

$$FC_{aeroPM10} = \frac{ln\left(\frac{D_{aeroPM10}}{D_+}\right)}{ln\left(\frac{D+}{D_-}\right)} \tag{16}$$

Where $D_{aeroPM10}$ stands for the geomtetric diameter corresponding to aerodynamic PM10 (for dust $D_{aeroPM10} = 6.8$ $\mu m$), and $D_+$ and $D_-$ correspond to the upper and lower limit of the model size bin straddling over $D_{aeroPM10}$ (in the TM4 case, $D_+ = 10$ $\mu m$ and $D_- = 2.5$ $\mu m$ ).

As the stations are located very close to the emission regions, we can expect some unusual peak in the observations. In order to exclude unwanted outliers from the datasets, we apply a rolling mean of 3 hours, which coincide with the metereology

timestep of the online version of the model. Applying a rolling mean is a way to dampen the higher frequency components of the signal, smoothing out fast fluctuations and point up the general trend.

As noted by Jasper&all in [55], the obervations might overall overestimate the true values, as we cannot exclude the contribution of other tracers to total $PM_{10}$, and because filtering the concentration according to wind direction leads means to restrict our datset to the most dust-rich air masses.

## 5.2   Validation method

For each station, we initially plotted the superimposed timeseries of the dust concentration measurements, the offline model output and the online one (see figures 17 - 24). These graphs allow to easily understand the overall model performance, and they are particularly suitable to qualitatively evualuate the model performance in reproducing the seasonality of the dust emission and transport paths.
For a more quantitative analysis, we did a scatter plot of the models monthly outputs against the corresponding measurements and fitted it to a linear relationship:

$$observation = \boldsymbol{\alpha} + \boldsymbol{\beta} \cdot model \tag{17}$$

In fact, in the ideal case, the relationship between modelled and measured concentrations would be a line passing through the origin of the axes ($\alpha = 0$) and with the slope $\beta$ equal to 1. The deviation of the linear fit from this line provides us with quantitative information about the model performance:

$\boldsymbol{\alpha} > 1$ and $\boldsymbol{\beta} > 0$: the model overestimates the observations at all scales

$\boldsymbol{\alpha} > 1$ and $\boldsymbol{\beta} < 0$ : the model overestimates the observations at large scale
and underestimate them at small scale

$\boldsymbol{\alpha} < 1$ and $\boldsymbol{\beta} > 0$: the model overestimates the observations at small scale
and underestimate them at large scale

$\boldsymbol{\alpha} < 1$ and $\boldsymbol{\beta} < 0$: the model underestimates the observations at all scales

For each linear fit, we additionally calculated the following parameters: the Pearson correlation coefficient, the root mean squared difference, the mean bias, and the

standard deviation. The meaning and the mathematical formulation of each parameter is explained as follow ($O_i$ always refers to an observation and $M_i$ to the corresponding modelled value):

**Pearson correlation coefficient** $\quad r = \dfrac{\sum_{i=1}^{N}(M_i - \overline{M})(O_i - \overline{O})}{\sqrt{\left[\sum_{i=1}^{N}(M_i - \overline{M})\right] \cdot \left[\sum_{i=1}^{N}(O_i - \overline{O})\right]}}$

This is a unitless parameter that quantifies the strenght of the linear correlation between the observed and the modelled quantity, or in other words how well the modelled pattern matches the observed pattern. The better the flutuations of the modelled dust follow the fluctuations of the observed one, the higher will be the correlation coefficient. In the ideal case, $r = 1$ and the relationship between the two quantities is linear.

However, this coefficient provides information only about the relative behavoir of the two quantities, and it is not useful to quantify the discrepancy between the two. For this purpose, we calculate the root mean square difference and the mean bias.

**Root mean squared difference RMSD**: $\quad \sqrt{\dfrac{\sum_{i=1}^{N}[M_i - O_i]^2}{N}}$

The RMSD quantifies the amplitude of the fluctuation between the model and the observations. In the ideal case in which the model and the observations coincide in each point, the RMSD would be equal to zero. As a general rule, the higher the RMSD, the worse is the model performance. As the difference between modelled and observed value appears squared in the formula, this parameter is particularly sensitive to the outliers. The RMSD has the same unit as the observed quantity (in our case $\mu grams/m^3$).

**mean BIAS**: $\quad \frac{1}{N}\sum_{i=1}^{N}(M_i - O_i) = \overline{M} - \overline{O}$

the mean BIAS represents the average difference between the model and the observations. As for the RMSD, the mean bias has the same unit as the observed quantity: in our case, it will represent the average difference in $\mu grams/m^3$ between the modelled dust load and the observed dust load.

**standard deviation $\sigma$**: $\quad \sqrt{\dfrac{\sum_{i=1}^{N}(x_i - \overline{x})^2}{N}}$

where $x_i$ is an element of a dataset and $\overline{x}$ its average. The standard deviation measures

the dispersion of the data around its average value. If the data follow a gaussian distribution, $\sigma$ represents the width of the gaussian. Note that while in the definition of the previous paramteres the values of $M_i$ and $O_i$ appeared mixed in the equations, on the contrary $\sigma$ quantifies the internal variability of a dataset and is calculated independently for each of them: the station data, the online model the offline one (ath the locations of the observations).

In this context, $\sigma$ is not of straightforward interpretation. The dispersion of a dataset can be due to two overlapping factors: an error in correctly modelling the dust load, or in measuring it for the observations dataset, and an intrinsic fluctuation of the observed phenomena due to its seasonal cycle and changes in the windfields.

In general, the closer the model $\sigma$ to the observed one, the better it reproduces the observed distribution.

### 5.2.1   Taylor graph

In order to graphically summarize the change in the model performance when using online dust emissions instead of offline ones, we plotted the results of the validation in a Taylor diagram[59]. The Taylor diagram is usually used to make models performance intercomparison when dealing with multiple complex models, such those used in climate science and Earth system modelling.

Using this diagram, the correlation coeffcient, the root mean squared difference and the standard deviation are summarized in one single point on a 2D plot, providing a visual representation of how well the model-simulated field resemble the observed field.

The points are represented in polar coordinates on a polar style graph. The standard deviation is plotted on the radial dimension, and the radial distance of the point form the origin is proportional to the value of $\sigma$. The correlation coefficient is plotted on the angular coordinate, and the correlation coefficient is equal to the cosine of the azimuthal position of the point. As the correlation of the observation with itself is by definition 1, the obervation point thus alway lies on the horizontal axes ($0°$ azimuth), respecting the relation $cos(0°) = 1$.

A family of concentric circles centered in the observations point is added to the diagram to plot the root mean squared difference RMSD. The model RMSD is proportional to

the radial distance between the model point and the observation point. The smaller the RMSD, the closer the model point to the observation point, and the inner the circle of the family the model point is contained in.

See figure 26 for the Tayor diagram of this validation.

## 5.3 The validation results

### 5.3.1 The timeseries

The timeseries for each station of the model-simulated dust concentration and the observed one are plotted in figures 17 - 24.

The performance of the two versions of the TM4-ECPL is overall good. Note that the only two stations where the atmospheric dust load was directly measured are Miami (figure 17) and Barbados (figure 18). For the other stations, the dust load is calculated inderectly from the total atmopsheric $PM_{10}$ with the different methodologies explained in the previous section.

In general, the seasonality of the dust emissions and the transport seems to be well captured by both versions of the model for most of the stations. The stations which shows the worse correspondence between model and observation are Bambey and Mbour. These two stations are located in the same model grid and were subject to the most severe data post-processing due to their proximity to the coast, which lead to the interference of sea-salt in the same diameter range as dust in the total $PM_{10}$.

The station of Barbados, even if the seasonality is fully captured, is massively overestimated by both version of the model. This behaviour might be justified by the fact that this station falls on the left edge of model box, and is located on the horizontal plume of dust crossing the Atlantic Ocean. As a consequence, the gradient of dust concentration along the horizontal direction of the grid might be quite strong, the dust concentration being higher on the right edge of the grid and lower on the left edge of the grid. As the model gives as an output the dust concentration averaged over all the gridcell, the modelled dust concentration in this grid will be higher than the real value measured at a location situated on the left of the grid, as for Barbados.
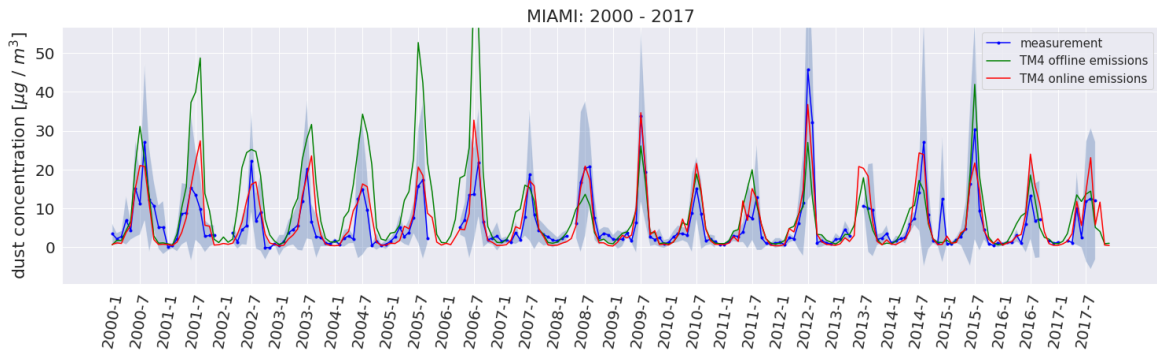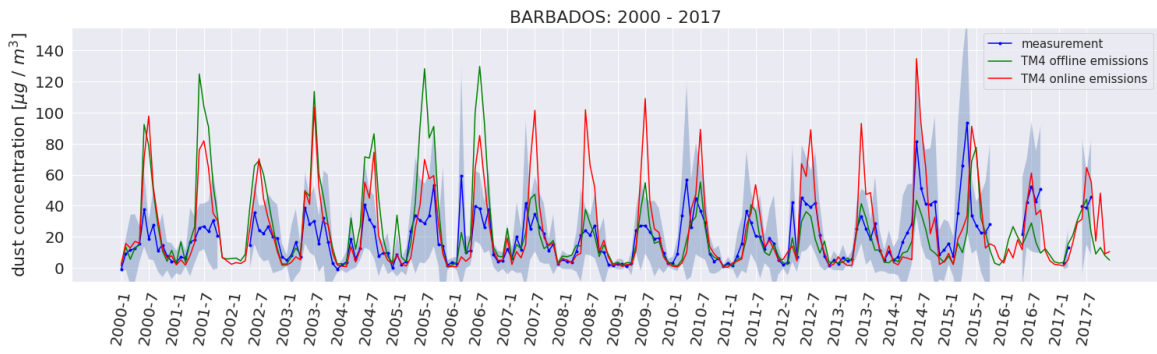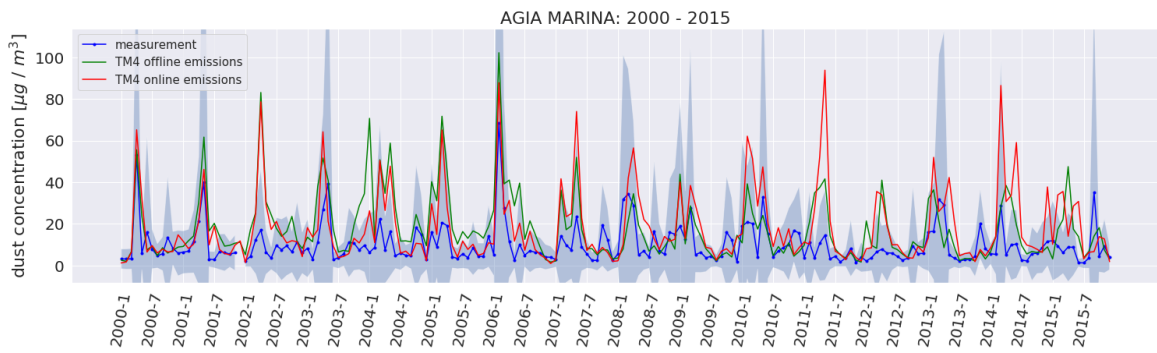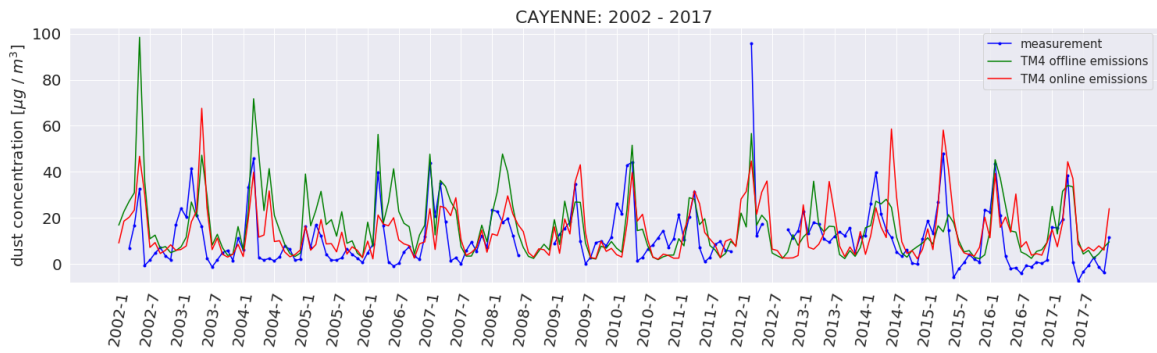
35

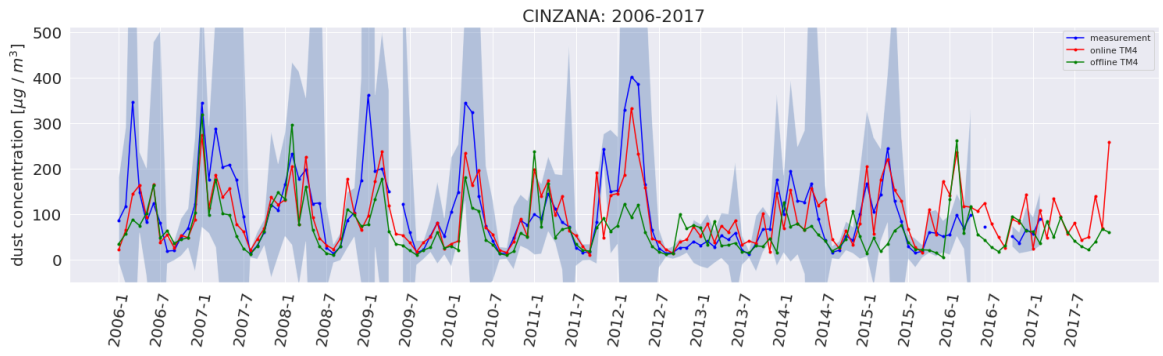Figure 17



Figure 18



Figure 19
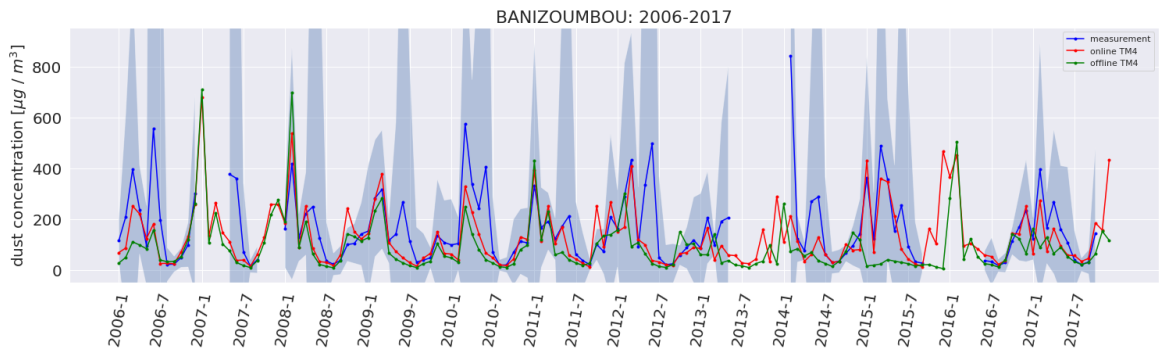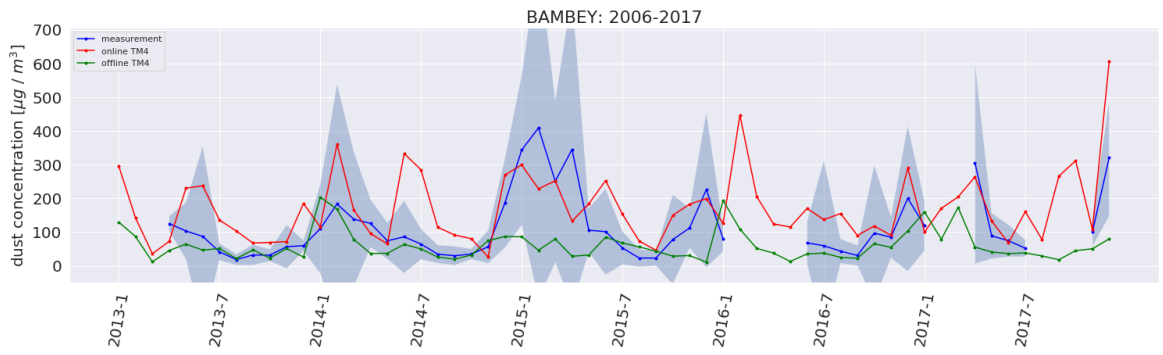


Figure 20

Figure 21



Figure 22



Figure 23
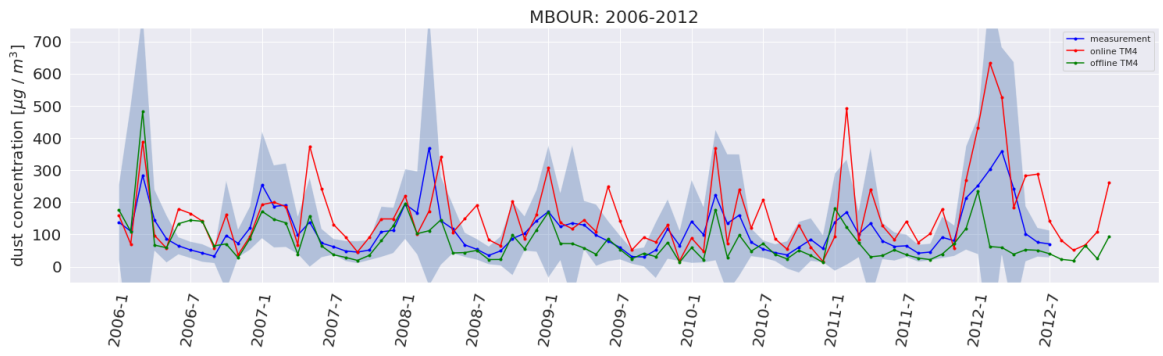


Figure 24

Figures 2-9: *Timeseries of the observed and modelled dust concentration at the 8 stations. The shaded area corresponds to the observation standard deviation. In Miami and Barbados, the standard deviation of the monthly avergae is reported in the datasets. In Agia Marina and all the African station, the datasets reported a daily and 5-minutes output respectively, and the standard deviation is calculated as internal flutuation of the data. For the sation of Cayenne, the data reported the monthly output alone without any associated error. The red line depicts the output of the online version of the model, the green one the offline one.*

### 5.3.2 The scatter plots

A quantitative comparison between the performance of the two TM4-ECPL versions is represented by the scatter plots in figure 25 . For both versions of the model, the model-simulated dust concentrations are plotted against the correspoinding observations, in both linear and logarithmic scale.

In linear scale it is easier to appreciate the performance of the model linear fit to a 1:1 line, while in logarithmic scale it is easier to grasp the model performance at different scales.

From the linear plots in figure 25 (left column), we can see that the offline version of the model overall underestimate the observed atmospheric dust load,particularly for the stations near the emission sources (green dots). The best linear fit slope is of 0.71 and 0.37 for the online and offline version, respectively.

The online version also performs better in terms of the total mean bias, resulting in a mean bias of 2.58 $\mu g/m^3$, better of one order of magnitude with respect to the mean bias of -14.27 $\mu g/m^3$ of the offline version. If compared to the total average dust load observed at the slected locations of approximately 51 $\mu g/m^3$, the online mean bias corresponds to the 5% of the total load, and the offline mean bias corresponds to the 30% of the total load.

The use online emissions also results in a sligthly better correlation coefficient: the online version of the model shows a correlation of $r = 0.75$ with the observations, while the offline version shows a correlation of $r = 0.61$.
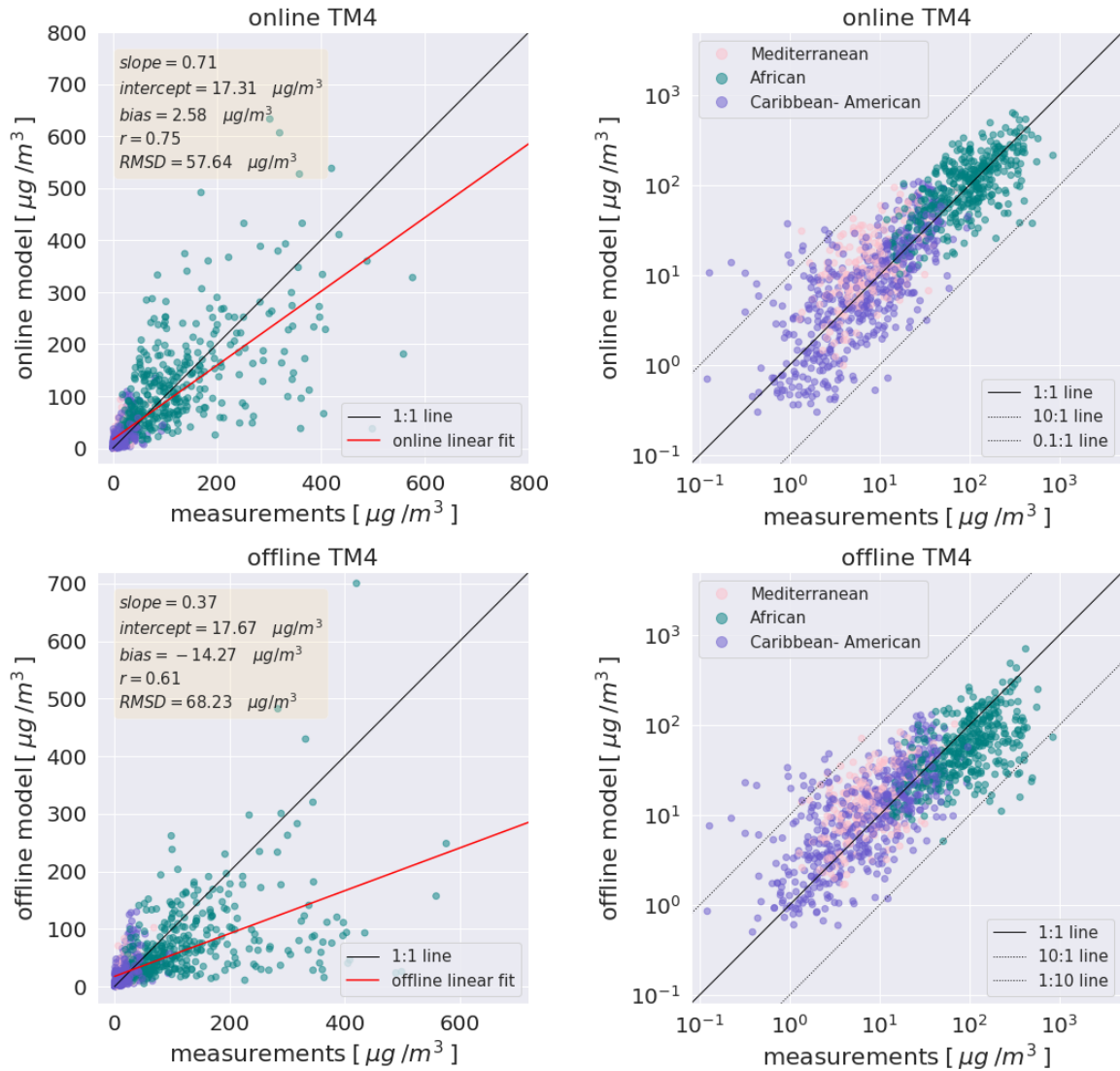
Figure 25: *Monthly averaged observed dust concentration versus the model-simulated dust concentration at the same locations in µg/m³. On the left column, the scatterplots are plotted in linear scale, on the right column in log scale. In the linear scale plots, the 1:1 line is plotted in black, and the best linear fit in red (online TM4), and orange (offline TM4). The text box reports, for each graph, the slope and the intercept of the linear fit, the mean bias, the Pearson correlation coefficient (r) and the centered root mean squared error (RMSD). In the log scale plots, the black line is the 1:1 line, and the dashed lines are the 10:1 and 1:10 lines. In all plots, the stations are geographically grouped: African stations (M'bour, Bambey, Cinzana, Banizoumbou) are plotted in green, the stations on the American coasts and in the Carribbean (Miami, Barbados, Cayenne) are plotted in violet, and the only Mediterranean station (Agia Marina) is plotted in pink.*

On the right column of figure 25 the scatterplots are plotted in logarithmic scale. The symmetric dashed lines are the 10:1 line and the 1:10, which enclose the area of the plot in which the points are within an order of magnitude distance from the 1:1 line. As dust emissions are still quite uncertain, the one order of magnitude distance from the 1:1 line is usually taken as a reference when validating natural dust[60]. In this sense, both versions of the model perform quite good, as only a few outliers are not comprised between the two dashed lines. We can see that the offline version of the model tends to underestimate the dust concentration at large scale, near the emissions region (green dots in the scatterplots), but overall performs better than the online version at small scale.

From these scatterplots, we can infere that, when it comes to reproducing dust emissions, the online emission scheme performs better than the offline one. When it comes to stations far from the sources (the violet dots in the scatterplots), the discrepancy between model and observation can be due to other physical-chemical processes, such transport or deposition mechanisms. However, the good accordance between the online emission scheme and the observations near the sources, where transport and deposition come into play more marginally, suggests that the online emission scheme reproduces better the dust emissions than the offline one. We can also notice that the online emissions scheme predicts emissions of one order of magnitude higher than the offline one, which, on the contrary, seem to underestimate them of one order of magnitude.

### 5.3.3 The Taylor diagram

The Taylor diagram that summarizes the change in the TM4-ECPL model performance when using an online emissions scheme instead of an offline one is plotted in figure 26.

From the Taylor diagram, we can conclude that the use of the online emission scheme slightly improve of the model performance with respect to the three plotted parameters. There is a 15% improvement in the correlation coefficient (from 0.61 to 0.75), meaning that the seasonality of the dust emission and of the transport routes is probably better captured.

The root mean squared error RMSD decreased of about 11 $\mu$g/m$^3$ (from 68 $\mu$g/m$^3$ to 57 $\mu$g/m$^3$), which corresponds to the 21% of the avearage observed dust load of 51

40

$\mu g/m^3$.

The standard deviation of the online emissions scheme gets much closer to the observed one with respect to the offline one. In fact, the observations show a standard deviation of 84 $\mu g/m^3$, the concentrations simulated with the online scheme at the same locations show a standard deviation of 79 $\mu g/m^3$, and 51 $\mu g/m^3$ for the offline one. This means that the distribution of the offline-modelled concentrations around their mean is much more skewed than the distribution observed in the measurements.

As we said in the previous section, the dispersion of the observed values might be due to both a real variabilty of the phenomena, or to observation error or error in the retrival of the dust fraction from the total $PM_{10}$.



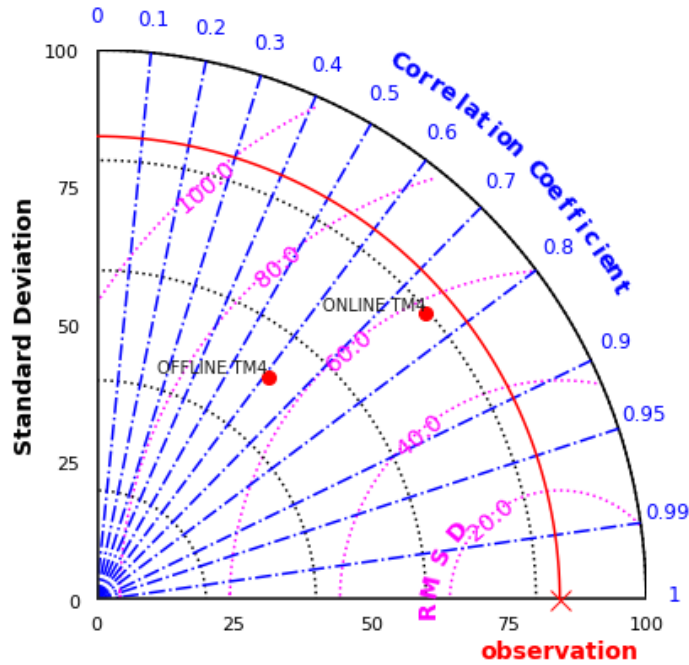Figure 26: *Taylor diagram comparing the overall performance of the offline and the online dust emissions scheme in the TM4-ECPL model. The diagram compares the Pearson correlation coefficient (on the polar angle coordinate), the standard deviation in $\mu g/m^3$ (on the radial coordinate),and the root mean squared distance RMSD in $\mu g/m^3$ (as distance from the observation point) of the two model versions*

41

# 6 The case of study: dust effects over air quality in the Mediterrenean basin

We aim to use the TM4-ECPL to assess the impact of natural dust on air quality in cities of the Mediterranean basin. The Mediterranean area is significanlty affected by the transport of natural dust, as result of its proximity to the Saharan and Middle Eastern sources and its dry climate, which favours the long lifetime of suspended aersols.

The initial aim of this study was to address the impact of natural dust on the air quality of large, densely populated cities. The Mediterranenan basin hosts only two megacities (i.e. with a population of more than 10 million inhabitants): Cairo and Instanbul. In this study, we also included Rome and Barcelona as representative of the West side of the basin, and Athens and Lemesos as representative of the East side of the basin. It should be noted that the highest urban concentration of the East part od the basin are found outside of the European Union, but getting atmospheric data from those location it is often not trivial. The location of Lisbon was added to check for dust intrusions outside of the basin.

The European Monitoring and Evaluation Programme (EMEP) and Aerosols, Clouds and Trace Gases Research Infrastructure (ACTRIS) provide a wide set of timeseries of PM10 measurements for multiple years and locations. Our initial intention was to identify from the timeseries of the measured PM10 the days in which the European limits for particulate matter have been exceedeed, use the TM4-ECPL to do a speciation of the PM10 peaks and calculate from the speciation the dust fractional contribution to the exceedance. However, the comparison between measured and simulated daily PM10 at selected locations showed the presence of anoumalous peaks in the modelled field, which surpasses sometimes by an order of magnitude the measured ones. Figure 27 shows the comparison between the measured PM10 field and the modelled one in Barcelona for the year 2014. We can notice how the timeserie of modelled and measured PM10 are, in general, in good accordance, but that most of the EU limit exceedances predicted by the model do not find a correspondance in the data, and that the model peaks are dominated by dust. This same behaviour was found at different

Mediterranean locations. As our analysis aimed particularly at studying peaks and the dust fractional contribution to those, we decided to do a second validation of total PM10 restricted to the Mediterranean region.
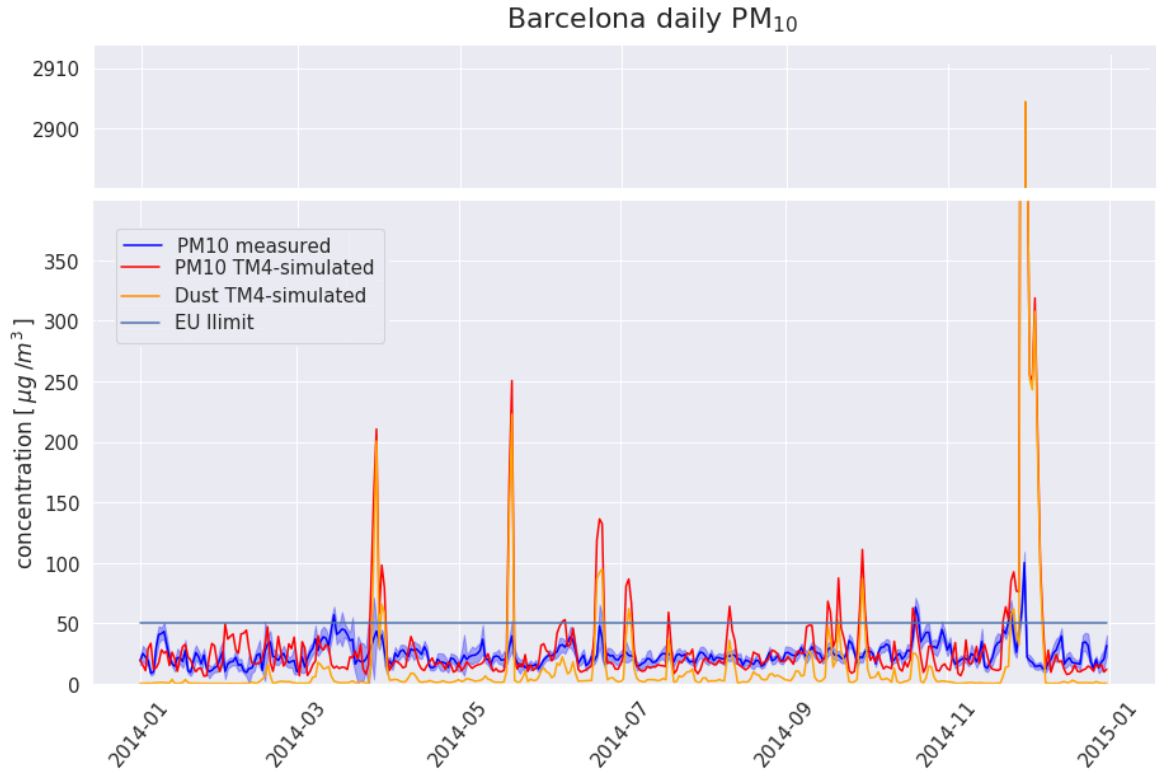


Figure 27: Timeseries of the measured PM10 (blue), modelled PM10 (red), and modelled dust (orange) for the year 2014 in Barcelona. The horizontal line is set at the EU limit of 50 µg/m³ for PM10 over a 24h avergaing period

## 6.1 PM10 validation and PM10 speciation in the Mediterranean region

The model validation for the total PM10 in the Mediterranean region aims at addressing two questions: if the model performs differently across the basin and, where there's a significant discrepancy between model and observations, which PM10 species are causing it.

To perform the validation, we run the TM4-ECPl model with 3-h temporal resolution using the online dust emission scheme for the years 2011-2017. The total PM10 field simulated by the TM4 - ECPL can be calculated as the summation of all the

43

individual atmospheric species belonging to this size range. In the speciation, we divided these atmospheric species in 5 categories: inorganic aersols, organic aerosols, biogenic aerosols, natural dust and sea salt, as reported in table 2 in the "Methods" section.

### 6.1.1  The locations and PM10 datasets choice

The locations used for the PM10 validation are listed in table 3. The initial choice for the stations location was the proximity to densely populated cities in the Mediterranean basin and the proximity to the dust sources. Stations data where initially taken from the EMEP (European Monitoring and Evaluation Programme) inventory, which provides the data of air pollutants concentrations reported yearly to the EEA (European Economic Area) by memberstates. This inventory contains PM10 timeseries starting from the year 2013 at major European cities.

Due to the significant discrepancy between measurements and model at most of the selected EMEP locations, we decided to add a few locations from the ACTRIS (Aerosols, Clouds and Trace gases Research Infrastructure) data inventory to check the consistency of the validation results. In particular, the two Actris stations in the south of Italy (Lamezia Terme and Lecce) were added to double check the bad performance of the model in this part of the Mediterranean basin, which emerged from the analysis of the Catania EMEP station. For Cyprus, the EMEP data have been integrated with the data from the study Pikridas&all (2018), provided by prof. M. Vrekoussis. All locations used for the validation are listed in table 3.

### 6.1.2  Measurements - model comparison on yearly averages

The daily PM10 timeseries (as in figure 27), suggested that the model performance is overall good and that the main discrepancy between model and observation is restricted to the peaks. As a first step to validate this hypothesis, we compared the yearly averages of the model output and the observations at different Mediterranenan locations. The result is depicted in figure 28.

From figure 28 we can notice that on an yearly average the model performs generally good across the basin, a part from stations located in the south of Italy, where the

| station | country | lat | lon | project acronym | years |
|---------|---------|-----|-----|-----------------|-------|
| Lisbon | Portugal | 38.73 | -9.14 | EMEP | 2013-2017 |
| Barcelona | Spain | 41.39 | 2.15 | EMEP | 2013-2017 |
| Rome-Naples | Italy | 41 | 13.5 | EMEP | 2013-2017 |
| Montelibretti | Italy | 42.10 | 12.63 | ACTRIS-EMEP | 2011-2015 |
| Catania | Italy | 37.5 | 15.09 | EMEP | 2015-2017 |
| Lamezia Terme | Italy | 38.88 | 16.23 | GAW-WDCA | 2015-2017 |
| Lecce | Italy | 40.33 | 18.12 | GAW-WDCA | 2015-2017 |
| Lemesos | Cyprus | 35 | 34.5 | EMEP | 2014-2017 |
| Cyprus (various*) | Cyprus | 34.7 | 33 | Pikiridas&all (2018) | 2011-2015 |
| Athens | Greece | 37.98 | 23.73 | EMEP | 2013-2017 |
| Cairo | Egypt | 30.08 | 31.29 | GAW-WDCA | 2011-2014 |

Table 3: *Stations used for the PM10 validation. For each stations, it is reported: the city name where the stations are located, the country, the latitude and the longitude, the project acronyms the data are associated with, and the years for which the data are available. Rome and Naples, Agia Marina and Lemesos are reported together beacuse they fall in the same box grid and the reported coordinates are those of the center gridbox.*

measured values are significanlty below the modelled ones. In general, the model tends to slightly over-estimate the yearly measured value, except for the station closer to the dust emissions (Cairo).

### 6.1.3 PM10 validation on monthly averages

In order to understad whether the seasonal variability of the PM10 is well enough captured by the model, we performed a validation of the monthly total PM10 concentration following the same procedure as for the validation of natural dust in Section "Validation of the online dust emission scheme". We averaged the measurement data, which have a daily resolution, and compared it with the speciated PM10 load calculated from the monthly averaged output of the TM4-ECPL. The timeseries are represente in figures 29 - 31. For each timeserie, the measurements and the model values are represented
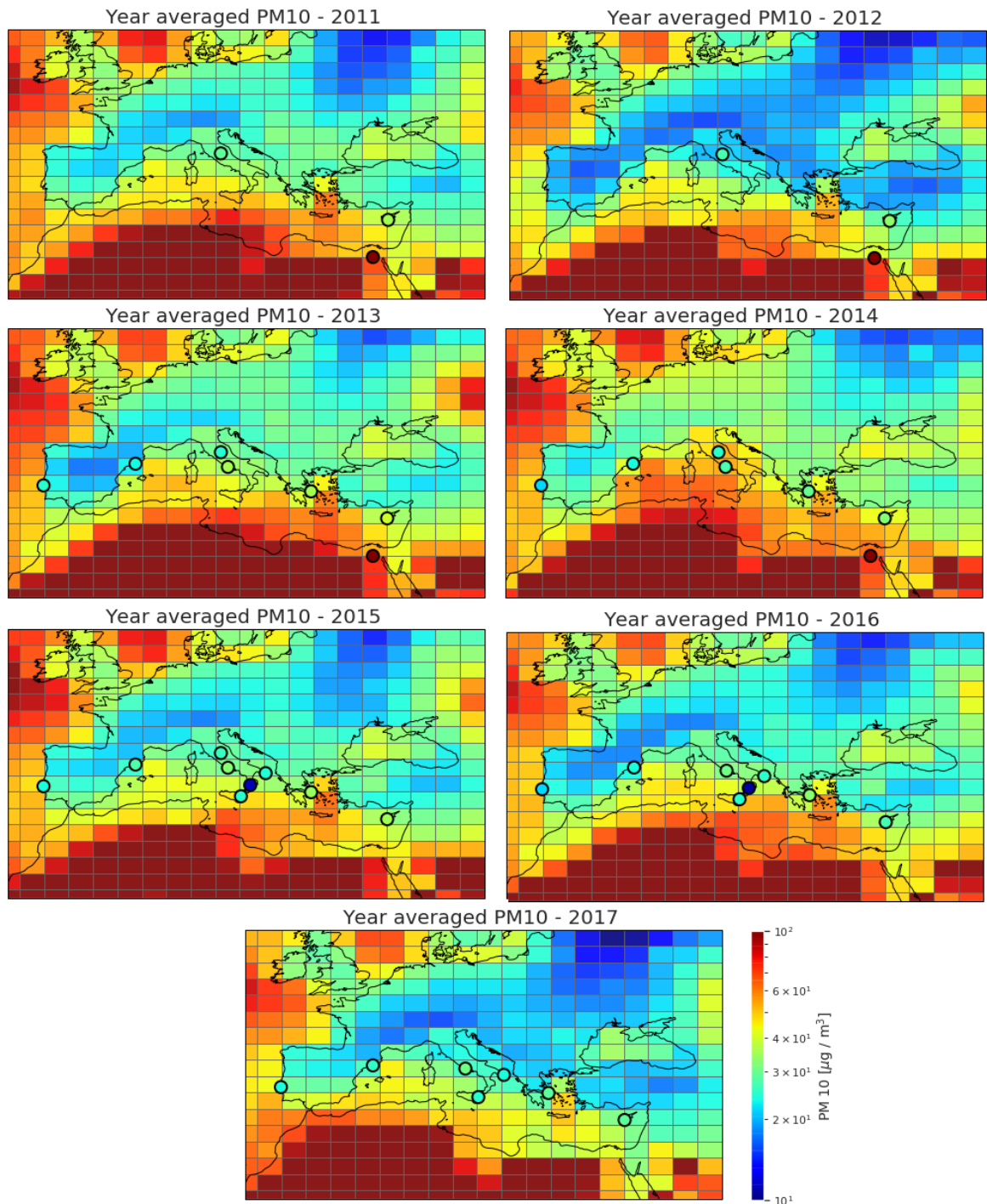
Figure 28: Yearly averaged PM10 fields modelled by the TM4-ECPL model compared with yearly averaged PM10 measurements at selected Mediterranean locations.

in a scatterplot. For each scatterplot, we performed a linear fit and calculated the Pearson correlation coefficient, the mean bias and the root mean squared error as we did for the previous validation.
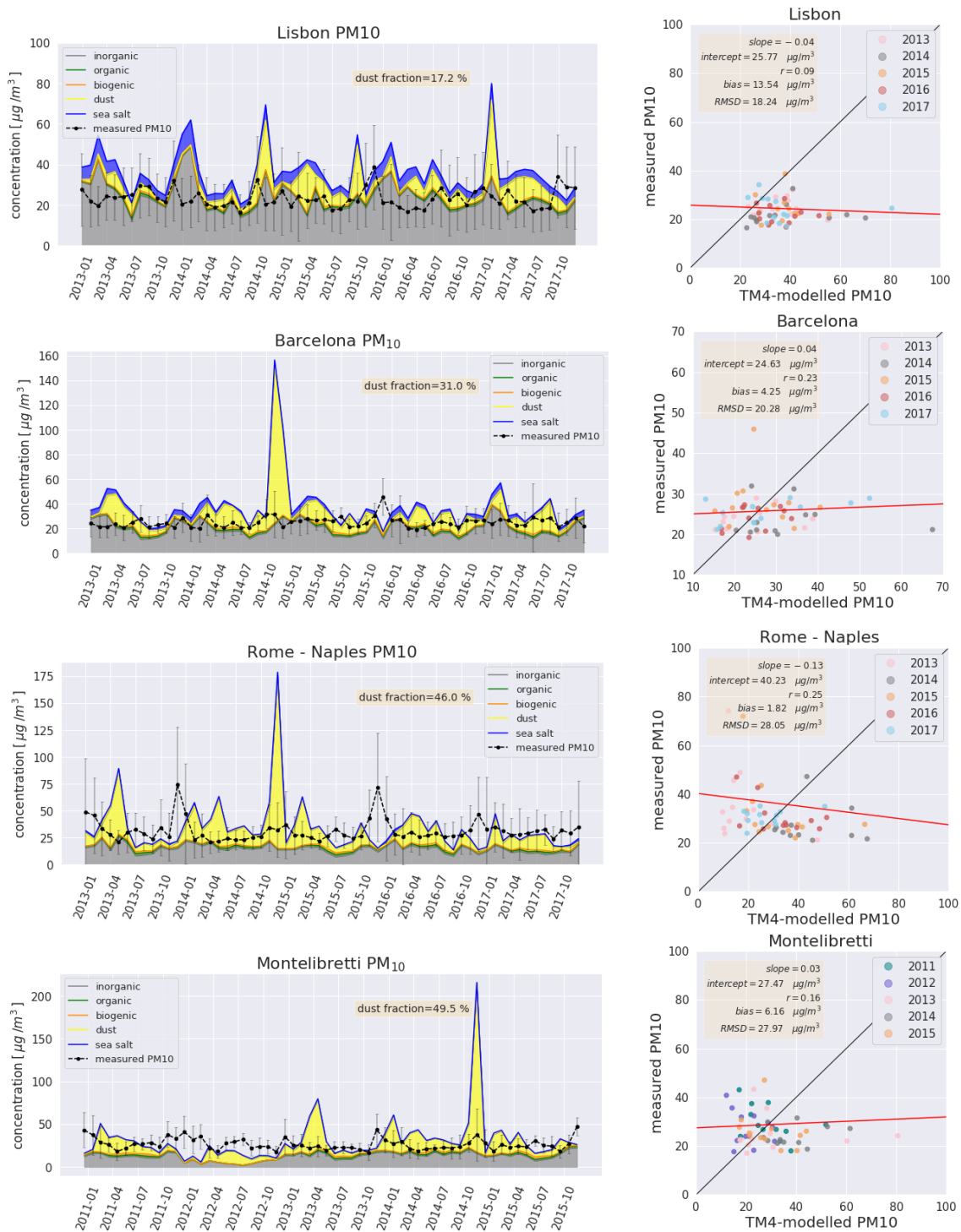
Figure 29: *Left: timeseries of the modelled PM10 speciation as compared to measurements at the locations of Lisbona, Barcelona, Rome-Naples, Montelibretti. Measurements are reported with the corresponding monthly standard deviation. The dust fraction over the entire modelled timserie is reported in the textbox. Right: measurements-model scatterplots at each location. Model values are reported on the x-axis and the corresponding measurements on the y-axis. The linear fit parameters (slope and intercept), the Pearson correlation coefficient, the mean bias and the root mean sqaured error for each scatterplot is reported in the text-box.*
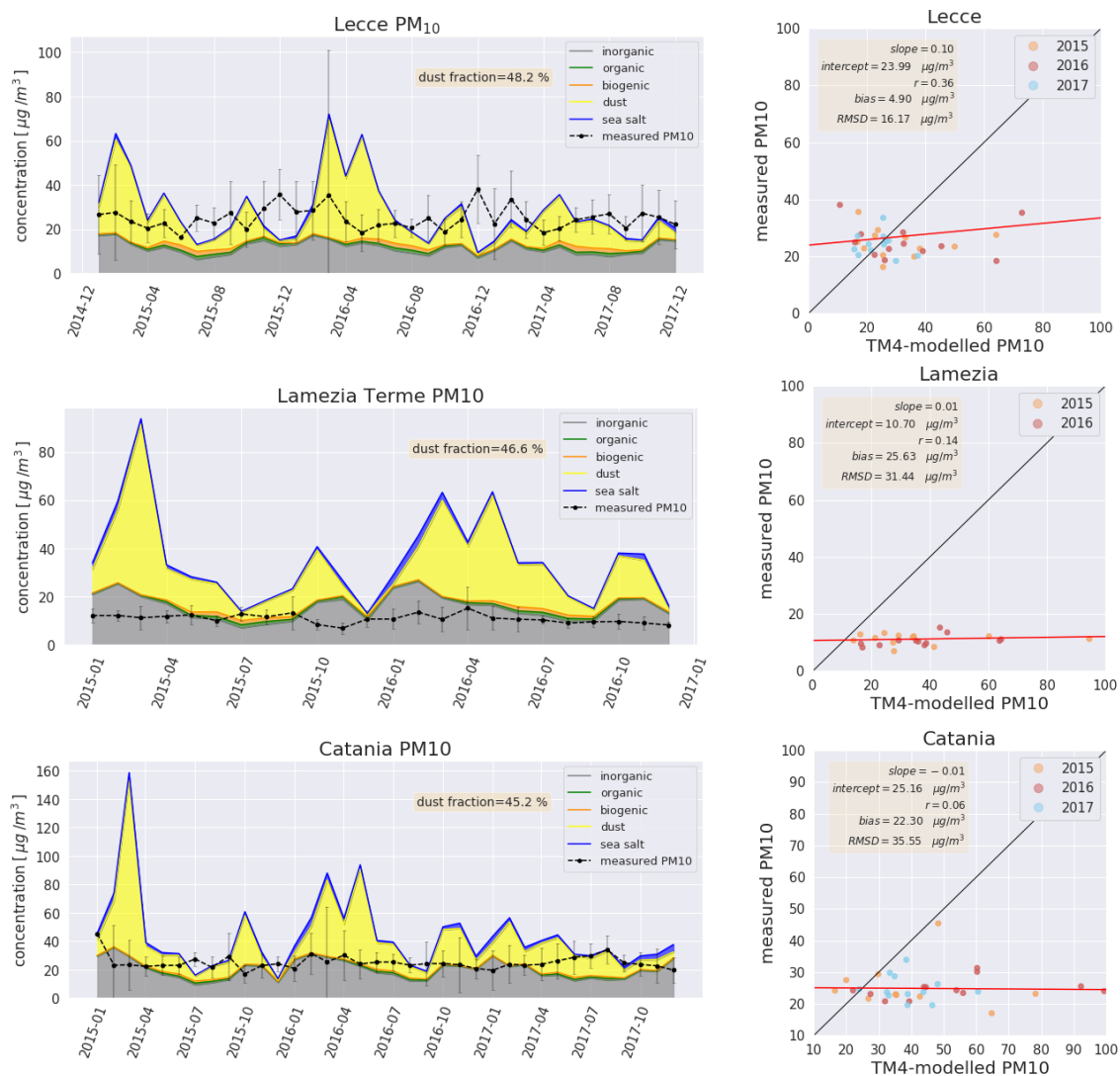
Figure 30: *Left: timseries of the modelled PM10 speciation as compared to measurements at the locations of Lecce, Lamezia Terme, and Catania. Measurements are reported with the corresponding monthly standard deviation. The dust fraction over the entire modelled timserie is reported in the textbox. Right: measurements-model scatterplots at each location. Model values are reported on the x-axis and the corresponding measurements on the y-axis. The linear fit parameters (slope and intercept), the Pearson correlation coefficient, the mean bias and the root mean sqaured error for each scatterplot is reported in the text-box.*
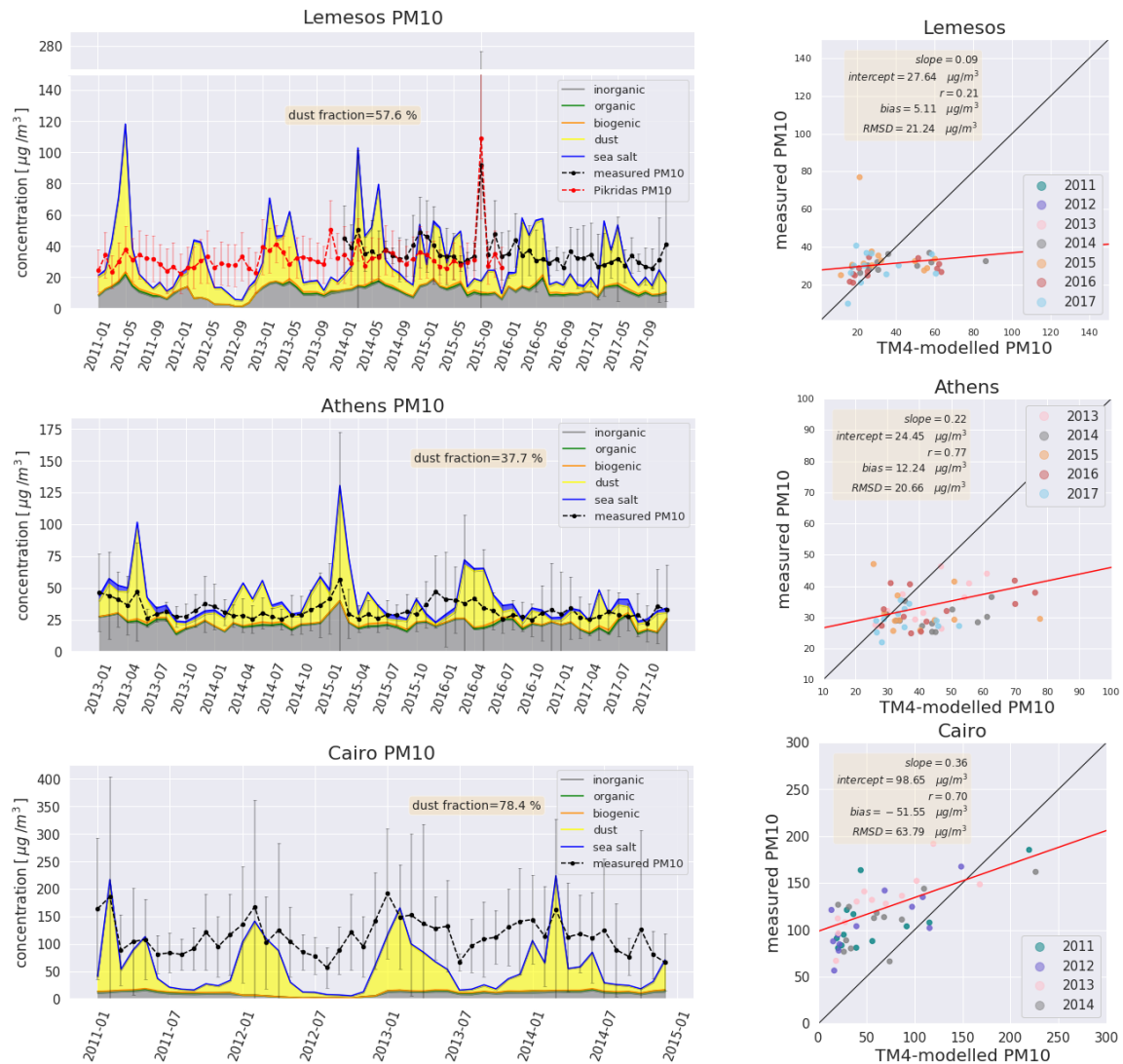
Figure 31: *Left: timseries of the modelled PM10 speciation as compared to measurements at the locations of Athens, Cyprus, and Cairo. Measurements are reported with the corresponding monthly standard deviation. The dust fraction over the entire modelled timserie is reported in the textbox. Right: measurements-model scatterplots at each location. Model values are reported on the x-axis and the corresponding measurements on the y-axis. The linear fit parameters (slope and intercept), the Pearson correlation coefficient, the mean bias and the root mean sqaured error for each scatterplot is reported in the text-box.*

### 6.1.4   Discussion of PM10 validation results

In general, the timeseries in figure 29, 30 and 31 suggest that the model performance is better on the East side of the basin than on the West side. For all stations, the linear fit over the scatterplot data is far from the 1:1 line, the fit slope being close to 0 for most station. In all stations except from Cairo, the presence of wide fluctuations in the modelled PM10 load, in general not observed in the data, tends to flatten out the linear relation. These wide fluctuations predicted by the model seem quite uniformly due to dust: in all stations, the PM10 speciation reveals that dust and inorganic aerosols are the most abudant component of the total PM10 load, and dust seasonal fluctuations dominate the peaks in the modelled PM10 timeseries everywhere except from Lisbon, which is the only station located outside of the Mediterranenan basin.

The location of Rome-Naples sticks out as the worst, showing a negative linear relation between modelled and observed values.

**The East side of the basin:**

The best accordance between model and observation is achieved in Cairo, where the seasonality and the peaks of the PM10 measurements is almost fully captured. The two timeseries here show a relatively high Perason correlation coefficient of $r = 0.70$. This result is in good accordance with the result of the dust validation, which showed that the dust concentration near the sources is well modelled by the TM4-ECPL with the online emissions scheme. However, the model here is quite significanlty underestimating the measured PM10: the calculated negative bias of -51 µg/$m^3$ accounts for roughly half of the yearly average at this location (around 100 µg/$m^3$).

The model performs fairly also at the location of Athens. Here the seasonality seems to be fairly captured, scoring a Pearson coefficient of $r = 0.77$. While the overall PM10 timeserie is well captured by the model, the model is overestimating the PM10 peaks.

Always on the East side of the basin, in the station of Cyprus the model performs fairly on the total average, having a low bias of 5.11 µg/m³ between model and obervation. However, the observed PM10 field is rather constant around 30 µg/m³ and shows, a part from one significant peak, only mild fluctuation around the average, while the modelled field shows much stronger seasonal fluctuations, leading to a flat linear

relation (slope = 0.09).

**The West side of the basin:**

The west side of the basin shows quite uniformely a bad correlation between model and observations.

In the region of south of Italy the validation was performed over three station: Lecce, Lamezia Terme and Catania. In the stations of Lamezia Terme and Catania the modelled PM10 concentration are significantly above the measurements, the bias being in both cases around the double than the averaged measured field. Morevore, the model predicts seasonal fluctuations which are totally absent in the data (resulting ina a correlation of $r = 0.14$ for Lamezia Termena and $r$=0.06 in Catania). However, the for these stations, the measurements do not appear totally trustable: over a time lapse of multiple years, the measures remain almost constant and show a very low variability (in particular the Lamezia Terme data). This appear quite implausable for two stations located in the middle of the Mediterranean and realtively close to the Saharan dust sources. In order to understand weather the PM10 measurements at this stations reflect the real status of the atmosphere, we checked for the AOD timeserie at the location of the stations. Figures 32 and 33 show the area-averaged timeseries of the Aerosol Optical Depth at 550 nm as measured by the NASA MODIS Spectroradiometer at both locations for the years 2015-2017.

Both AOD timeseries show a significant seasonal variabilty, showing spring and summer maximums. This suggests the presence of an inconsistency between the ground PM10 measurements and the AOD data. The presence of spring maximums characterize also the modelled PM10 timeseries, suggesting that a better correlation between model and measurements might be obtained performing the validation using AOD data. However, one must remember that the AOD is a measure of the total amount of aerosols in the vertical atmospheric column, so a further analysis would be needed to assess whether the AOD peaks also resulted in a surface concentration peak, or if the aerosol plume passed at an high altitude and did not affect dramatically the surface concentration. Nevertheless, aerosol lidar measurements performed over the timespan between 2014 and 2017 reported numerous Saharan dust events in this region[61]. As there are concrete reasons to mistrust the PM10 data, a further analysis should be carried on at
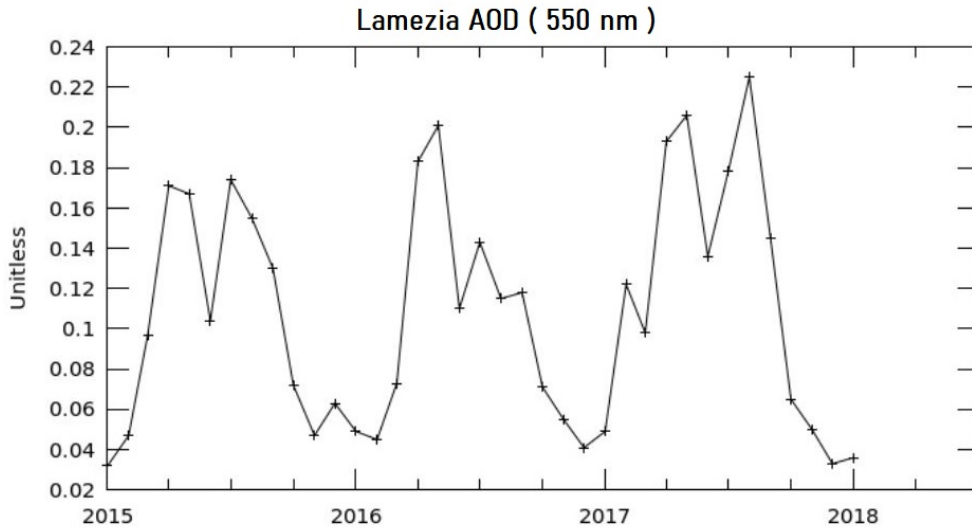
Figure 32: *Time series of the area-averaged Aerosol Optical Depth at 550 nm, with monthly temporal resultion and 1° spatial resolution, measured by MODIS-Aqua between January 2015 - January 2018, in the area [15.5E, 38N, 17.5E, 40N]*
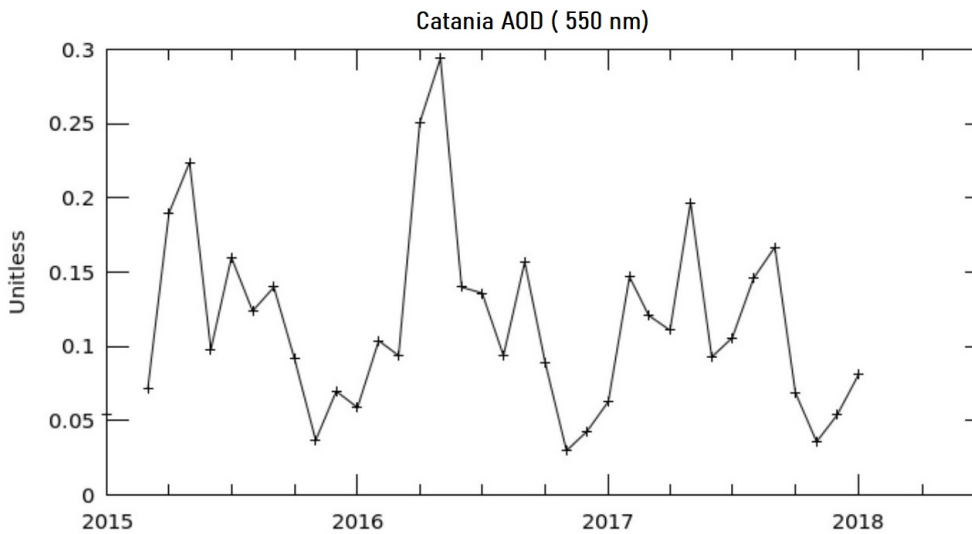


Figure 33: *Time series of the area-averaged Aerosol Optical Depth at 550 nm, with monthly temporal resultion and 1° spatial resolution, measured by MODIS-Aqua between January 2015 - January 2018, in the area [14.5E, 36.8N, 15.7E, 38N]*

these locations in order to validate the model performance in reproducing the PM10 field.

The at the location of Lecce the model performs better than in Catania and Lamezia Terme. Model and measurements correlate slightly better ($r = 0.36$), and the bias is

significantly lower (4.9 $\mu$g/m$^3$).

In the stations of Barcelona, Rome-Naples and Montelibretti the model validation leads to similar results.The modelled signal tends to follow the measured one when the PM10 concentration is low, but fails to grasp fluctuations: most PM10 peaks predicted by the model are not present in the measurements, and the measured PM10 peaks are often not reproduced by the model (particularly in the Rome timeserie). This results in a relatively low bias (between 1.82 and 6.16 $\mu$g/m$^3$), but in a low correlation (between 0.16 and 0.25) and flat slopes of the best linear fits.

The station of Lisbon is the only which is not located in the Mediterranean basin and that faces the open Atlantic Ocean. Here the speciation of the PM10 timeserie is different from the other locations: the PM10 load is dominated by inorganic aerosols, the fractional contribution of sea salt is higher than at the other locations and dust's fractional contribution is significanlty lower. A further speciation of the inorganic aerosols at this location revealed that the major contribution to this PM10 component comes from particulate water, which are water droplets containing debris. The validation result seem to suggest that at this location the model overestimates particulate water, as the modelled inorganic aerosol concentration alone surpasses the measured one. At this station, the model and measured field are uncorrelated, showing a correlation coefficient of $r = 0.09$ and linear fit slope of -0.04.

### 6.1.5  Overall conclusions on PM10 validation

The result of the model validation suggests that the TM4-ECPl model with the online dust emission scheme performs better at reproducing the PM10 concentration field on the East side of the basin than the West side. However, as some surface PM10 concentrations proved to be not trustworthy, a second validation using AOD measurements would be needed to better assess the model performance in the entire basin. For each timeseries, the dust fractional contribution to the total PM10 load has been calculated from the speciation, and is reported in text for each timeserie. Overall, the general trend of the dust field along the basin seems to be captured by the model, showing an overall increasing trend from West to East (from 17% in Lisbon to 57% in Cyprus), and from North to South, peaking in Cairo (78%).

However, we cannot ignore the fact that the result of the PM10 validation in the basin is overall extremely poor. The low correspondance between model and observation might be due to an intrinsic overestimation of dust in the dust emissions. However, the online emission scheme perfomed quite good at simulating the dust concentration near the dust sources (see figures 21 - 24 in the section "Validation of the dust emission schemes"), and this behaviour is confirmed by the good result in the PM10 validation in Cairo (where the model is actually underestimating the total PM10 field). The reason of the bad performance in the simulation of the model PM10 field might thus be sought in the deposition fluxes and removal processes. However, a further analysis would be of need to understand which process is driving the anomalous dust load fluctuations.

As a last test to assess the goodness of the model performance in the basin, we decided to confront the modelled PM10 fields with the PM10 measurements data from Pikiridas&all (2018), which represent a fully troustable set of PM10 measurements for the years under study.

### 6.1.6   Model performance in Cyprus

We dispose of a trustworthy PM10 measurements multi-years timeserie for the location of Cyprus, used in the study by Pikridas&all (2018)[62].
These PM10 measurements were conducted using a TEOM (Tapered Element Oscillating Microballance measurements) and gravimetric analysis of particulate matter at 7 different stations located on the island over the period 1998-2015. In the same study, the timeserie of dust concentration was calculated for the same period using the Querol method[25]. The comparison between the model PM10 yearly averages and the yearly averages measured in this study are reported in table 4, while the same comparison for dust is reported in table 5.

From the results reported in table 4, we can see that the yearly average of modelled PM10 is always compatible with the measured value within the measurement standard deviation, except for the year 2014. The two values are always compatible within the model standard deviation, which is always quite high, accounting for half or more of the modelled average value, implying that the model predicts wide PM10

| year | PM10 TM4-ECPL | PM10 Pikridas(2018) |
|---|---|---|
| 2011 | $(36 \pm 31)\ \mu\text{g/m}^3$ | $(25 \pm 9)\ \mu\text{g/m}^3$ |
| 2012 | $(26 \pm 12)\ \mu\text{g/m}^3$ | $(33 \pm 10)\ \mu\text{g/m}^3$ |
| 2013 | $(34 \pm 19)\ \mu\text{g/m}^3$ | $(39 \pm 8)\ \mu\text{g/m}^3$ |
| 2014 | $(48 \pm 28)\ \mu\text{g/m}^3$ | $(38 \pm 9)\ \mu\text{g/m}^3$ |
| 2015 | $(34 \pm 16)\ \mu\text{g/m}^3$ | $(41 \pm 10)\ \mu\text{g/m}^3$ |

Table 4: *Yearly average of the TM4-ECPL PM10 as compared to the measured one in Cyprus as in Pikradis&all (2018). The model standard deviation are computed from the monthly output fields, the measurements standard deviation from the yearly average measured at different stations*

| year | Dust TM4-ECPL | Dust Pikridas(2018) |
|---|---|---|
| 2011 | $(20 \pm 27)\ \mu\text{g/m}^3$ | $(6 \pm 4)\ \mu\text{g/m}^3$ |
| 2012 | $(12 \pm 10)\ \mu\text{g/m}^3$ | $(5 \pm 2)\ \mu\text{g/m}^3$ |
| 2013 | $(18 \pm 16)\ \mu\text{g/m}^3$ | $(12 \pm 11)\ \mu\text{g/m}^3$ |
| 2014 | $(26 \pm 24)\ \mu\text{g/m}^3$ | $(8 \pm 7)\ \mu\text{g/m}^3$ |
| 2015 | $(16 \pm 12)\mu\text{g/m}^3$ | $(9 \pm 8)\ \mu\text{g/m}^3$ |

Table 5: *Yearly average of the TM4-ECPL dust as compared to the calculated one in Cyprus as in Pikradis&all (2018). The model standard deviation are computed from monthly output fields, the Pikradis one from the monthly estimates of dust*

fluctuations between different months (as could already be seen in figure 31). From the results reported in table 5, it is clear that the model tends to overestimate the dust concentration. The modelled average value is always 2-3 times higher than the Pikridas one. The two values are compatible within the Pikridas standard deviation only for the years 2015 and 2013.

## 6.2 Exceedances computation in Mediterranean cities

The 3h - 3°×2° runs were used to compute the number of daily exceedances of the EU limit in 6 cities of the Mediterranenan basin over a time range of 3 years (2015 - 2017). We selected Barcelona, Rome, Athens, Lemesos, Cairo and Instanbul as the citites of interest. Instanbul was included because it is one of the few megacities (i.e. population > 10 million) of the Medierranean basin, the only other being Cairo. Even if we did not perform the PM10 validation directly in the Instanbul area because of the lack of data, the validation result was overall fair in the nearby stations.

In general, the model seems to capture the seasonality of dust events in the Mediterranenan basin. All locations on the East side of tha basin (Athens, Lemesos, Instanbul, Cairo) show a peak in the number of exceedances during Spring, while locations on the West side show a peak between Spring and Summer. The fractional contribution of dust to the yearly exceedances oscillate around a 45%-55% on the West side of the basin and around 45%-65% over the East side (excluding Cairo), and the number of exceedances increases from West to East and moving closer to the dust sources. Cairo register the higher number of yearly exceedances with a dust contribution between 70%-75%.

State members are allowed to surpass without penalties the EU daily PM10 limit-value of 50 µg/m$^3$ only 35 times a year. We included in these limitations also not EU cities (Cairo and Instabul), as the 50 µg/m$^3$ daily limit is set by the World Health Organization. Our model predicted that the limit was not met for all years and locations under consideration. The results are contanined in tables 6 - 11.

### 6.2.1 Comparison with previous exceedences studies

We confronted the results listed in tables 6 - 11 with previous studies of exceedances in the Mediterranenan basin. No study reported the number of > 50µg/m$^3$ daily exceedances for the years and locations we analyzed, so it is not possible to make a direct comparison. However, as dust events show a periodic cycle, it is still possible to draw some conclusions on the reliability of our results.

A recent study[63] estimated desert dust contribution to the PM10 load in different Mediterranenan countries between the years 2015-2018. They estimated an average

dust concentration of (8.8 ± 7.5), (7.5 ± 5.5), (9.0 ± 5.6) µg/m³ in Spain, Italy and Instanbul respectively. At the locations of Barcelona, Rome and Instanbul averaging the daily dust timeserie of the TM4-ECPL output, we obtain an average yearly dust concentration of (9± 21) µg/m³, (11± 33) µg/m³, (12 ± 34) respectively, in good accordance with the previous study's results.

The same study[63] estimated the typical PM10 concentration range during dust outbreaks, which are selected as days in which a thershold value of 150µg/m³ is surpassed. They find that over the year 2015-2017 the PM10 load during dust outbreaks fluctuated between [213 - 327] µg/m³ in Spain and [153 -445] µg/m³ in Turkey. If we apply the same 150µg/m³ limit to our timeseries in Barcelona and Instanbul and calculate the average dust concentration during the dust outbreaks between 2015 and 2017 we get 208 ± 61 µg/m³ for Barcelona 246 ± 129 µg/m³ for Instanbul. Thus, both minimum and maximum values of TM4-ECPL simulated dust along the Mediterranean basin are in good accordance with this previous study.

When it comes to the number of estimated exceedances, the number predicted by the TM4-ECPL seems fair. Another study on PM10 exceedances conducted on the island of Crete[5], in the middle of the basin, found that in Crete daily EU PM10-limits are typically surpassed around 1 out of 5 days at background stations, which would correspond to roughly 70 exceedances per year. In 2011, a EEA technical report documented that, for the year 2009, Cyprus, Spain, Greece, and Italy, reported, respectively, 112, 35, 76 and 75 exceedances due to natural events.

The TM4-ECPL predicts a number of exceedances ranging between 36 and 44 in Barcelona, 51 and 74 in Rome, 61 and 85 in Athens, 59 and 79 in Lemesos, 46 to 67 in Instanbul, 73 and 103 in Cairo. We can conclude that the number of daily exceedances of the PM10 EU-limit predicted by the TM4-ECPL seem reasonable.

| Barcelona | | | | |
|---|---|---|---|---|
| **Year** | **Season** | **N° of exceedances** | **Average PM10 [$\mu$g/m$^3$]** | **Dust %** |
| **2015** | Winter | 1 | 44.35 | 0.5% |
| | Spring | 20 | 85 ± 40 | 60.4% |
| | Summer | 10 | 78 ± 26 | 68.6% |
| | Autumn | 5 | 127 ± 112 | 51.7% |
| | **yearly total** | **36** | 85 ± 34 | 45.3% |
| **2016** | Winter | 9 | 55± 27 | 25.1% |
| | Spring | 11 | 53 ± 12 | 52.3% |
| | Summer | 13 | 83 ± 45 | 64.7% |
| | Autumn | 8 | 86 ± 47 | 57.2% |
| | **yearly total** | **41** | 69 ± 17 | 49.8% |
| **2017** | Winter | 13 | 95 ± 64 | 28.8% |
| | Spring | 5 | 74 ± 43 | 58.8% |
| | Summer | 26 | 86 ± 33 | 73.0% |
| | Autumn | 0 | n.a. | n.a. |
| | **yearly total** | **44** | 85 ± 10 | 53.6% |

Table 6

| Rome | | | | |
|---|---|---|---|---|
| **Year** | **Season** | **N° of exceedances** | **Average PM10 [$\mu$g/m$^3$]** | **Dust %** |
| **2015** | Winter | 11 | 80± 31 | 62.3% |
| | Spring | 27 | 101 ± 131 | 55.4% |
| | Summer | 3 | 68 ± 10 | 70.4% |
| | Autumn | 17 | 79 ± 56 | 47.8% |
| | **yearly total** | **58** | 82 ± 14 | 58.9% |
| **2016** | Winter | 14 | 64± 16 | 16.6% |
| | Spring | 24 | 109± 90 | 59.2% |
| | Summer | 21 | 66± 23 | 58.2% |
| | Autumn | 15 | 64± 23 | 43.6% |
| | **yearly total** | **74** | 76 ± 23 | 44.4% |
| **2017** | Winter | 15 | 97± 58 | 29.7% |
| | Spring | 11 | 80± 49 | 40.8% |
| | Summer | 19 | 73± 22 | 64.9% |
| | Autumn | 6 | 48± 6 | 31.3% |
| | **yearly total** | **51** | 75 ± 20 | 41.7% |

Table 7

| Athens | | | | |
|---|---|---|---|---|
| Year | Season | N° of exceedances | Average PM10 [$\mu$g/m$^3$] | Dust % |
| **2015** | Winter | 28 | 156 ± 219 | 45.5% |
| | Spring | 29 | 108 ± 112 | 66.9% |
| | Summer | 7 | 55 ± 13 | 52.8% |
| | Autumn | 17 | 75 ± 37 | 44.6% |
| | **yearly total** | **81** | 85 ± 34 | 45.3% |
| **2016** | Winter | 18 | 71± 47 | 17.9% |
| | Spring | 43 | 131 ± 202 | 59.8% |
| | Summer | 13 | 68 ± 21 | 63.4% |
| | Autumn | 11 | 72 ± 60 | 47.0% |
| | **yearly total** | **85** | 85 ± 30 | 47.0% |
| **2017** | Winter | 21 | 60 ± 18 | 27.6% |
| | Spring | 18 | 91 ± 71 | 65.3% |
| | Summer | 12 | 66 ± 20 | 67.2% |
| | Autumn | 10 | 80 ± 30 | 52.7% |
| | **yearly total** | **61** | 74 ± 14 | 53.2% |

Table 8

| Lemesos | | | | |
|---|---|---|---|---|
| Year | Season | N° of exceedances | Average PM10 [$\mu$g/m$^3$] | Dust % |
| **2015** | Winter | 19 | 87± 41 | 55.2% |
| | Spring | 33 | 83 ± 66 | 69.7% |
| | Summer | 15 | 75 ± 61 | 67.1% |
| | Autumn | 12 | 57 ± 18 | 72.3% |
| | **yearly total** | **79** | 76 ± 13 | 66.1% |
| **2016** | Winter | 11 | 60± 20 | 38.8% |
| | Spring | 33 | 118± 77 | 72.5% |
| | Summer | 18 | 84± 39 | 65.5% |
| | Autumn | 5 | 46± 5 | 68.7% |
| | **yearly total** | **67** | 77 ± 32 | 61.6% |
| **2017** | Winter | 9 | 50 ± 7 | 40.6% |
| | Spring | 36 | 94 ± 93 | 70.7% |
| | Summer | 6 | 84 ± 15 | 74.4% |
| | Autumn | 8 | 71 ± 36 | 65.5% |
| | **yearly total** | **59** | 75 ± 18 | 62.8% |

Table 9

| Cairo | | | | |
|---|---|---|---|---|
| Year | Season | N° of exceedances | Average PM10 [$\mu$g/m$^3$] | Dust % |
| **2015** | Winter | 38 | 281 ± 460 | 78% |
| | Spring | 37 | 133 ± 130 | 78% |
| | Summer | 14 | 101 ± 82 | 75% |
| | Autumn | 14 | 67 ± 22 | 70% |
| | **yearly total** | **103** | 146 ± 94 | 75% |
| **2016** | Winter | 23 | 267 ± 446 | 68% |
| | Spring | 48 | 178 ± 201 | 82% |
| | Summer | 17 | 69 ± 19 | 69% |
| | Autumn | 4 | 52 ± 20 | 64% |
| | **yearly total** | **92** | 141 ± 100 | 71% |
| **2017** | Winter | 18 | 172 ± 223 | 72% |
| | Spring | 41 | 170 ± 252 | 78% |
| | Summer | 7 | 90 ± 24 | 79% |
| | Autumn | 7 | 92 ± 44 | 71% |
| | **yearly total** | **73** | 131 ± 46 | 75% |

Table 10

| Instanbul | | | | |
|---|---|---|---|---|
| Year | Season | N° of exceedances | Average PM10 [$\mu$g/m$^3$] | Dust % |
| **2015** | Winter | 21 | 113± 119 | 58% |
| | Spring | 31 | 86 ± 62 | 62% |
| | Summer | 8 | 52 ± 11 | 44% |
| | Autumn | 4 | 50 ± 6 | 47% |
| | **yearly total** | **64** | 75 ± 30 | 53% |
| **2016** | Winter | 4 | 56± 18 | 13% |
| | Spring | 27 | 125± 91 | 78% |
| | Summer | 12 | 56± 10 | 48% |
| | Autumn | 3 | 52± 4 | 45% |
| | **yearly total** | **67** | 77 ± 32 | 61.6% |
| **2017** | Winter | 4 | 50 ± 7 | 40.6% |
| | Spring | 27 | 94 ± 93 | 70.7% |
| | Summer | 12 | 84 ± 15 | 74.4% |
| | Autumn | 3 | 71 ± 36 | 65.5% |
| | **yearly total** | **46** | 72 ± 35 | 46% |

Table 11

# 7 Limitations encountered

## 7.1 Model limitations

The main model limitation encountered in this study was the spatial resolution. The model finest spatial resolution, $3° \times 2°$, allows us to calculate the atmospheric fields over a 300 km $\times$ 200 km grid-box, and we expect to find the better correlation with measurements around the center of the gridbox. If a city falls on the edge of a gridbox, the model fields might not be fully representative of the state of the atmosphere at that location, but rather at a point around 100 km far. This happened for example for the city of Lisbon, which sits on the left edge of a gridbox (see figure 34). In this



Figure 34: *Lisbon stations used for PM10 validation on the TM4-ECPL horizontal gridding*

particular case, the model gridbox center fall in the middle of the Atlantic Ocean, where the atmospheric composition is probably very different than in Lisbon. To mitigate this effect, the modelled atmospheric status in Lisbon has been computed as the average between the model gridbox and the nearby gridbox on the right. This have improved the correspondance between modelled and observed valued, but it is not a

accurate way of solving the issue. However, when it comes to natural dust transport, we expect the concentration gradients to be realively smooth. The use of a coarse spatial resolution should thus not affect dramatically the goodness of the modelled dust fields.

The relatively low spatial resolution might nevertheless affect the goodness of the simulated dust field. A recent paper by Kok&all (in pre-print at present) is suggesting that models with a spatial resolution in the order of 100 km are intrinsically ill-equipped to simulate the dust cycle. This foundamental limit would come from the fact that dust emission is extremely sensitive to the variation of climatological paramters such as wind speed and soil properties, a limitation that can only partially be overcome by sub-gridding of both parameters. The lack of solid high-resolution datasets also represent a challenge for an accurate dust emission simulation.

## 7.2   Limitations on the available dust data

A second limitation encountered is the absence of recent publicly available measurements of dust concentration. As we pointed out previously in this work, most stations measuring dust concentrations stopped being operative in the mid 1990, making the net of measuraments available for the validation of surface dust concentration fields extremely scarce. As reported in the Aerocom global dust model intercomparison[60], most models performs fairly in simulating the total atmospheric dust column, but great uncertainties are still present when modelling surface dust fields. The availability of recent dust concentration measurements would thus be of great importance to assess the models performance. For this study, it would have been of great importance the disposal of direct dust measurements in the Mediterranenan basin to perfom the surface dust validation.

# 8    Conclusions and future work

In this project, the TM4-ECPL chemistry and transport model has been succesfully validated for dust concentration in both its version using an *offline* dust emission scheme and an *online* dust emission scheme. The validation has been perfomed using recent surface dust concentration data at locations positioned at strategic locationd for the global dust transport. The result of the validation suggests that a moderate improvment in the model performance is obtained when using online emissions. In its offline version, the model shows a Pearson correlation coefficient of $r = 0.61$ with observations, a bias of -14.3 $\mu g/m^3$ and a linear correlaion with slope 0.37. In its online version all this parameters showed an improvemnt: $r$ goes up to 0.75, the bias lowers to 2.6 $\mu g/m^3$ and the linear correlation slope rises to 0.71.

The version of the TM4-ECPL using online dust emission has been used to study the impact on air quality in 6 cities of the Mediterranenan basin. In particular, the question we intented to answer is how many of the daily exceedances of the PM10 EU-limit are attributable to transport of natural dust from the North African and Middle Eastern dust sources. However, we encountered a potential weakness of the model when calculating the surface PM10 fields in the Mediterranenan area. Modelled and measured PM10 concentrations are essentially uncorrelated in most part of the basin. The correlation coefficient is always $r < 0.40$ and a the linear fit between model and measurements gives a flat slope, except for a few exeptions in the East part of the basin. The speciation on the PM10 monthly timeseries at the measurements locations suggests that the model predicts flucutations of the dust concentration which are much wider than the measured ones.

The confrontation of the PM10 and dust modelled concentration with a previous study by Pikridas&all (2018) in Cyprus[62] suggested that the model might over-estimate the yearly dust load in the Mediterranenan study by a factor between 2 or 3. However, the confrontation of the model results with a recent study of PM10 exceedances in the Mediterrenenan basin[63] by Gomez-Losada&all (2021) points in the direction that minimum and maximums average values of PM10 during dust outbreaks are well captured by the model.
Nethertheless, a more thorough analysis of the dust buget in the Mediterrenean basin

would be needed to understand which processes are leading to the model overestimation of the PM10 load.

The model output was used to estimate the number of daily exceedances of the PM10 EU-limit (set to 50 μg/m$^3$ over a 24-h averaging period) in 6 cities of the Mediterranenan basin: Barcelona, Rome, Athens, Lemesos, Cairo and Instambul. The model correcly predicts the seasoality of the number of exceedances, peaking in Spring anf Summer, and their increasing trend from West to East along the basin. The result seems plausible when compared to previous studies and data, but it cannot be considered fully trustable due to the proved poor performance of the model at simulating surface PM10

At present, we cannot exclude that the online dust emissions scheme might lead to an overestimation of the dust load in the Mediterranean region. The stations used for the dust field validation are in an excellent position to analyse the translatlantic dust transport. However, due to the absence of stations measuring dust concentration on the North African coast, we cannot exclude an overastimation of dust emission on that part of the dust sources. Another possibility would be an overestimation of the dust lifetime in the basin, due to an underestimation of deposition fluxes. These hypothesis would need to be checked, for example by using AOD data, which offer very good spatial coverage, to validate again the dust field, or by using deposition fluxes measurments, which would allow to check the goodness of the removal processes in the model.

The TM4-ECPL spatial resolution will be improved by LAMOS in the near future, downscaling it to 1°× 1°. As suggested by Kok&all (in pre-print)[55], improving the spatial resolution might enhance the performance of the online dust emissions scheme. However, according to Kok&all, 1°× 1° might be still too coarse to fully capture dust emissions.

# References

[1] D.W. Griffin, Atmospheric Movement of Microorganisms in Clouds of Desert Dust and Implications for Human Health. CLINICAL MICROBIOLOGY REVIEWS, p. 459-477, July 2007.

[2] N. Middleton, U. Kang. Sand and Dust Storms: Impact Mitigation. Sustainability. 2017.

[3] O. Alizadeh-Choobari, A. Sturman, P. Zawar-Reza. A global satellite view of the seasonal distribution of mineral dust and its correlation with atmospheric circulation. O. Alizadeh-Choobari, A. Sturman, P. Zawar-Reza. A global satellite view of the seasonal distribution of mineral dust and its correlation with atmospheric circulation. Dynamics of Atmospheres and Oceans, 68, 20-34. 2014.

[4] J. M. Prospero1, P. J. Lamb, African Droughts and Dust Transport to the Caribbean: Climate Change Implications. Science, vol 302. pages 1024-1027. November 2003.

[5] E. Gerasopoulos, G. Kouvarakis, P. Babasakalis, M. Vrekoussis, J.-P. Putaud, N. Mihalopoulos. Origin and variability of particulate matter (PM10) mass concentrations over the Eastern Mediterranean. Atmospheric Environment 40 (2006) 4679-4690.

[6] C. Mitsakou, G. Kallos, N. Papantoniou, C. Spyrou, S. Solomos, et al.. Saharan dust levels in Greece and received inhalation doses. Atmospheric Chemistry and Physics Discussions, European Geosciences Union, 2008, 8 (3), pp.11967-11996. hal-00304270

[7] U. Im, K. Markakis, M. Koçak, E. Gerasopoulos, N. Daskalakis, N. Mihalopoulos, A. Poupkou, T. Kindap, A. Unal, M. Kanakidou. Summertime aerosol chemical composition in the Eastern Mediterranean and ist sensitivity to temperature. Atmospheric Environment, Vol. 50, 164-173, 2012.

[8] X. Querol, J. Peya, M. Pandolfi, A. Alastuey, M. Cusack, N. Perez, T. Moreno, M. Viana, N. Mihalopoulos, G. Kallos, S. Kleanthous. African dust contributions

to mean ambient PM10 mass-levels across the Mediterranean Basin. Atmospheric Environment 43 (2009) 4266-4277.

[9] A. Slingo T. P. Ackerman R. P. Allan E. I. Kassianov S. A. McFarlane G. J. Robinson J. C. Barnard M. A. Miller J. E. Harries J. E. Russell S. Dewitte. Observations of the impact of a major Saharan dust storm on the atmospheric radiation balance. Geophys. Res. Lett. 33, L24817. 2006.

[10] C Richon, JC Dutay, F Dulac, R Wang. Modeling the impacts of atmospheric deposition of nitrogen and desert dust-derived phosphorus on nutrients and biological budgets of the Mediterranean Sea. Progress in Oceanography Volume 163, Pages 21-39, April 2018.

[11] V.H. Garrison, E.A. Shinn, W.T. Foreman, D.W. Griffin. African and Asian dust: from desert soils to coral reefs. BioScience 469. Vol. 53 No. 5. May 2003.

[12] J. Boy, W. Wilcke. Tropical Andean forest derives calcium and magnesium from Saharan dust. Glob. Biogeochem. Cycles 22, GB1027. 2008.

[13] C. A. Kellogg and D. W. Griffin. Aerobiology and the global transport of desert dust. TRENDS in Ecology and Evolution Vol.21 No.11. 2006.

[14] D. W. Dockery, C. A. Pope: Acute respiratory effects of particulate air pollution, Annu. Rev. Publ. Health, 15, 107 - 132, 1994

[15] L. Perez, A. Tobias, X. Querol, N. Kunzli, J. Pey, A. Alastuey, M. Viana, N. Valero, M. Gonzdlez-Cabre, J. Sunyer. Coarse Particles From Saharan Dust and Daily Mortality. Lippincott Williams & Wilkins. Epidemiology, Vol. 19, No. 6 (November 2008), pp. 800-807.

[16] D. Griffin, C. Kellogg, E. Shinn. Dust in the wind: long range transport of dust in the atmosphere and its implications for public and ecosystem health.Global Change Human Health. 2001;2:21-5.

[17] S. Nicholson. Land surface processes and Sahel climate. Rev. Geophys. 38, 117 (2000)

[18] Thomson, M. C., Molesworth, A. M., Djingarey, M. H., Yameogo, K. R., Belanger, F., and Cuevas, L. E.: Potential ofenvironmental models to predict meningitis epidemics in Africa, Trop. Med. Int. Health, 11(6), 781-788, 2006.

[19] European Environment Agency, EEA report No 10/2019 Air quality in Europe-2018 report.

[20] https://www.epa.gov/criteria-air-pollutants/naaqs-table

[21] World Health Organization. WHO Air quality guidelines for particulate matter, ozone, nitrogen dioxide and sulfur dioxide - Global update 2005 - Summary of risk assessment. 2006

[22] P. Ozer, M. B. O. M. Laghdaf, S. O. M. Lemine, J. Gassani. Estimation of air quality degradation due to Saharan dust at Nouakchott, Mauritania, from horizontal visibility data. Water Air Soil Pollut, 178:79-87. 2006

[23] S. Nava, S. Becagli, G. Calzolai, M. Chiari, F. Lucarelli, P. Prati, R. Traversi, R. Udisti, G. Valli, R. Vecchi. Saharan dust impact in central Italy: An overview on three years elemental data records. Atmospheric Environment 60. 2012.

[24] X. Querol, A. Alastuey, S. Rodriguez, M.M. Viana, B. Artinano, P. Salvador, E. Mantilla, S. Garcia do Santos, R. Fernandez Patier, J. de La Rosa, A. Sanchez de la Campa, M. Menendez. Levels of particulate matter in rural, urban and industrial sites in Spain. Elsevier. Science of the Total Environment 334 - 335 (2004) 359 - 376. 2004.

[25] M. Escudero, X. Querol, J. Peya, A. Alastuey, N. Perez, F. Ferreira,S. Alonso, S. Rodriguez, E. Cuevas. A methodology for the quantification of the net African dust load in air quality monitoring networks. Atmospheric Environment 41 (2007) 5516 - 5524.

[26] G. Kallos, A. Papadopoulos, P. Katsafados, S. Nickovic. Transatlantic Saharan dust transport: Model simulation and results. Journal of Geophisical Research, VOL. 111, D09204, 2006.

[27] B. Arvani, R. B. Pierce, S. Teggi, G. Ghermandi, L.Lombroso. Study of Saharan dust outbreak episode over the Po valley (northern Italy) using IDEA-international air quality forecast product. ProScience 1 (2014) 1-6.

[28] G. Kallos, A. Papadopoulos, O. Kakaliagou. A model for prediction of desert dust cycle in the atmosphere. Journal of Geophisical Research, vol. 106, no. D16 pages 18,113-18,129, August 27, 2001

[29] G. Kallos,P. Kassomenos, R.A. Pielke. Synoptic and Mesoscale Weather Conditions During Air Pollution Episodes in Athens, Greece. In: Kaplan H., Dinar N., Lacser A., Alexander Y. (eds) Transport and Diffusion in Turbulent Fields. Springer, Dordrecht (1993).

[30] I. Tegen, S. P. Harrison, K. Kohfeld, I. Colin Prentice, M. Coe, M. Heimann. Impact of vegetation and preferential source areas on global dust aerosol: Results from a model study. JGR, Vol. 107, No. D21, 4576. 2002.

[31] B. Marticorena and G. Bergametti. Modeling the atmospheric dust cycle: 1. Design of a soil-derived dust emission scheme. JGR, Vol. 100, No. D8, pag 16,415-16,430, August 20, 1995.

[32] B. Heinold, J. Helmert, O. Hellmuth, R. Wolke, A. Ansmann, B. Marticorena, B. Laurent, and I. Tegen. Regional modeling of Saharan dust events using LM-MUSCAT: Model description and case studies. Journal of Geophysical Research, VOL. 112, D11204, 2007.

[33] J. Helmert, B. Heinold, I. Tegen, O. Hellmuth, and M. Wendisch, On the direct and semidirect effects of Saharan dust over Europe: A modeling study. JOURNAL OF GEOPHYSICAL RESEARCH, VOL. 112, D13208, 2007.

[34] Li, L., Mahowald, N. M., Miller, R. L., PÃ©rez GarcÃa-Pando, C., Klose, M., Hamilton, D. S., GonÃ§alves Ageitos, M., Ginoux, P., Balkanski, Y., Green, R. O., Kalashnikova, O., Kok, J. F., Obiso, V., Paynter, D., and Thompson, D. R.: Quantifying the range of the dust direct radiative effect due to source mineralogy uncertainty, Atmos. Chem. Phys., 21, 3973-4005, 2021.

[35] Kok, J., Ridley, D., Zhou, Q. et al. Smaller desert dust cooling effect estimated from analysis of dust size and abundance. Nature Geosci 10, 274-278 (2017).

[36] Adebiyi, A. and Kok, J. Climate models miss most of the coarse dust in the atmosphere. Science Advances 08 Apr 2020: Vol. 6, no. 15.

[37] Cormier S., Lomnicki S., Backes W., Dellinger B. Origin and Health Impacts of Emissions of Toxic By-Products and Fine Particles from Combustion and Thermal Treatment of Hazardous Wastes and Materials. Environmental health perspectives 114(6):810-7. 2006.

[38] Stafoggia M., Zauli-Sajani, S. Pey, J. & all. Desert Dust Outbreaks in Southern Europe: Contribution to Daily PM10 Concentrations and Short-Term Associations with Mortality and Hospital Admissions. Environ Health Perspect 124:413-419. 2016.

[39] Crooks J. L., Cascio W. E., Percy M. S. The Association between Dust Storms and Daily Non-Accidental Mortality in the United States, 1993-2005. Environmental Health Perspectives, vol. 124, n. 11.2016

[40] J. Seinfeld, S.Pandis. Atmospheric chemistry and physics: from air pollution to climate change. Jhon Wiley & Sons.2016

[41] A.S. Goudie, N.J. Middleton. Desert Dust in the Global System. Springer. 2006.

[42] Global Assessment of Sand and Dust Storms. United Nations Environment Programme, Nairobi.UNEP, WMO, UNCCD (2016).

[43] Global Assessment of Sand and Dust Storms. United Nations Environment Programme, Nairobi.UNEP, WMO, UNCCD (2016).

[44] N. Mahowald, S. Albani, J. F. Kok, S. Engelstaeder, R. Scanza, D. S. Ward, M. G. Flanner. The size distribution of desert dust aerosols and its impact on the Earth system. Aeolian Research 15 (2014) 53-71.

[45] Brasseur G.P, Jacob D. J., Modeling of Atmospheric Chemistry. Cambridge Univeristy Press (2017).

[46] Myriokefalitakis S., Nenes A., Baker A. R., Mihalopoulos N., Kanakidou M. Myriokefalitakis, S., Nenes, A., Baker, A. R., Mihalopoulos, N., Kanakidou, M. (2016). Bioavailable atmospheric phosphorous supply to the global ocean: A 3-D global modeling study. Biogeosciences, 13(24), 6519-6543. 2016.

[47] Kaplan, J. O., Bigelow, N. H., Prentice, I. C., Harrison, S. P., Bartlein, P. J., Christensen, T. R., Cramer, W., Matveyeva, N. V., McGuire, A. D., Murray, D. F., Razzhivin, V. Y., Smith, B., Walker, D. A., Anderson, P. M., Andreev, A. A., Brubaker, L. B., Edwards, M. E., and Lozhkin, A. V. (2003 - in press). Climate change and arctic ecosystems II: Modeling, paleodata-model comparisons, and future projections. Journal of Geophysical Research.

[48] Zobler L. A world soil file for global climate modeling, Tech. Rep. NASA TM-87802, pp. 32 , NASA, Washington D.C., 1986

[49] F. Dentener, S. Kinne, T. Bond, O. Boucher, J. Cofala, S. Generoso, P. Ginoux, S. Gong, J. J. Hoelzemann, A. Ito, L. Marelli, J. E. Penner, J.-P. Putaud, C. Textor, M. Schulz, G. R. van der Werf, and J. Wilson. Emissions of primary aerosol and precursor gases in the years 2000 and 1750 prescribed data-sets for . Atmos. Chem. Phys., 6, 4321-4344, 2006

[50] Arimoto R., Duce R. A., Ray B. J., Ellis W. G., Cullen J. D., and Merrill J. T. Trace-Elements in the Atmosphere over the North-Atlantic, J. Geophys. Res.-Atmos., 100(D1), 1199-1213 (1995)

[51] Prospero, J. M.: The Atmospheric Transport of Particles to the Ocean, in: Particle Flux in the Ocean, edited by: Ittekkot, V., SchÂšafer, P., Honjo, S., and Depetris, P. J., John Wiley& Sons Ltd., New York (1996).

[52] A numerical study of the contributions of dust source regions to the global dust budget. Taichu Y. Tanaka, Masaru Chiba, Global and Planetary Change 52 88-104(2006)

[53] Zuidema P., Alvarez C., Kramer S. J., Custals L.,Izaguirre M., Sealy P., Prospero J. M., Blades E. Is summer African dust arriving earlier to Barbados? The Updated Long-Term In Situ Dust Mass Concentration Time Series from Ragged Point,

Barbados, and Miami, Florida Paquita. Bulletin of the American Meteorological Society, Vol. 100, Issue 10, pag. 1981-1986. 2019

[54] http://www.lisa.u-pec.fr/SDT/

[55] J. F. Kok, A. A. Adebiyi, S. Albani, Y. Balkanski, R. Checa-Garcia, M. Chin, P. R. Colarco, D. S. Hamilton, Y. Huang, A. Ito, M. Klose, D. M. Leung, L. Li, N. M. Mahowald, R. L. Miller, V. Obiso, C. Perez Garcia-Pando, A. Rocha-Lima, J. S. Wan, and C. A. Whicker. Improved representation of the global dust cycle using observational constraints on dust properties and abundance. In Pre-Print

[56] Climate Models and Remote Sensing Retrievals Neglect Substantial Desert Dust Asphericity. Huang, Y., et al., Geophys. Res. Lett. 47, (2020)

[57] O. Cavalieri, F. Cairo, F. Fierli, G. Di Donfrancesco, M. Snels, M. Viterbini, F. Cardillo, B. Chatenet, P. Formenti, B. Marticorena, and J. L. Rajot. Variability of aerosol vertical distribution in the Sahel. Atmos. Chem. Phys. Discuss., 10, 17609-17655, 2010.

[58] Joseph M. Prospero, Anne E. Barkley, Cassandra J. Gaston, Arthur Campos y Sansano, and Kathy Panecho. Characterizing and Quantifying African Dust Transport and Deposition to South America: Implications for the Phosphorus Budget in the Amazon Basin. Global Biogeochemical Cycles, 34 (2020)

[59] Summarizing multiple aspects of model performance in a single diagram. K. E. Taylor. JOURNAL OF GEOPHYSICAL RESEARCH, VOL. 106, NO. D7, PAGES 7183-7192, APRIL 16 2001.

[60] N. Huneeus, M. Schulz, Y. Balkanski, J. Griesfeller, J. Prospero, S. Kinne, S. Bauer, O. Boucher, M. Chin, F. Dentener, T. Diehl, R. Easter, D. Fillmore, S. Ghan, P. Ginoux, A. Grini, L. Horowitz, D. Koch, M. C. Krol, W. Landing, X. Liu, N. Mahowald, R. Miller, J.-J. Morcrette, G. Myhre, J. Penner, J. Perlwitz, P. Stier, T. Takemura, and C. S. Zender. Global dust model intercomparison in AeroCom phase I. Atmos. Chem. Phys., 11, 7781-7816 (2011).

[61] Soupiona, O., Papayannis, A., Kokkalis, P., Foskinis, R., SÃ¡nchez HernÃ¡ndez, G., Ortiz-Amezcua, P., Mylonaki, M., Papanikolaou, C.-A., Papagiannopoulos, N., Samaras, S., Gross, S., Mamouri, R.-E., Alados-Arboledas, L., Amodeo, A., and Psiloglou, B.: EARLINET observations of Saharan dust intrusions over the northern Mediterranean region (2014-2017): properties and impact on radiative forcing, Atmos. Chem. Phys., 20, 15147-15166

[62] M. Pikridas, M. Vrekoussis, J. Sciare, S. Kleanthous, E. Vasiliadou, C. Kizas, C. Savvides, N. Mihalopoulos. Spatial and temporal (short and long-term) variability of submicron, fine and sub-10 $\mu$m particulate matter (PM1,PM2.5,PM10) in Cyprus. Atmospheric Environment 191 (2018) 79-93.

[63] Gomez-Losada, A., Jose C. M. Pires, J. C. M. Estimation of Particulate Matter Contributions from Desert Outbreaks in Mediterranean Countries (2015-2018) Using the Time Series Clustering Method. Atmosphere 2021, 12, 5.

[64] Paschalidou, A.K.; Kassomenos, P.; Karanikola P.; Disaggregating the contribution of local dispersion and long-range transport to the high PM10 values measured in a Mediterranean urban environment. Science of the Total Environment 527-528 (2015) 119-125.